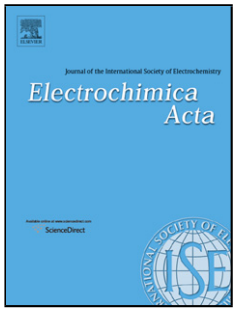

Title: A novel in-situ corrosion monitoring electrode for reinforced concrete structures

Authors: Subbiah Karthick, Velu Saraswathy, Seung-Jun Kwon, Han-Seung Lee, Rethinam Natarajan, Dong-Jin Park

PII: S0013-4686(17)32210-7
DOI: https://doi.org/10.1016/j.electacta.2017.10.088
Reference: EA 30474

To appear in: *Electrochimica Acta*

Received date: 3-9-2017
Revised date: 7-10-2017
Accepted date: 14-10-2017

Please cite this article as: Subbiah Karthick, Velu Saraswathy, Seung-Jun Kwon, Han-Seung Lee, Rethinam Natarajan, Dong-Jin Park, A novel in-situ corrosion monitoring electrode for reinforced concrete structures, Electrochimica Acta https://doi.org/10.1016/j.electacta.2017.10.088

A novel in-situ corrosion monitoring electrode for reinforced concrete structures

Subbiah Karthick [a,b], Velu Saraswathy[a,c] , Seung-Jun Kwon[d], Han-Seung Lee[a*], Rethinam Natarajan[b] and Dong-Jin Park[a]

[a] *Department of Architectural Engineering, Hanyang University, 1271 Sa 3-dong, Sangrokgu, Ansan 426791, Korea;*

[b] *PG and Research Department of Chemistry, Alagappa Government Arts College, Karaikudi 630003, Tamil Nadu, India;*

[c] *Corrosion and Materials Protection Division, CSIR-Central Electrochemical Research Institute, Karaikudi 630003, Tamil Nadu, India;*

[d] *Department of Civil Engineering, Hannam University, Daejeon 306-791, Korea;*

Corresponding author e-mail: ercleehs@hanyang.ac.kr; Tel.: +82-31-400-4181

Highlights:

- In-situ corrosion monitoring electrode based on Ce-doped $NiFe_2O_4$ was fabricated.
- The corrosion performance of the steel rebar was evaluated by using FCME in the simulated concrete environment without and with 3% NaCl.
- The corrosion behavior of the steel rebar was studied by using open circuit potential, AC-impedance, and potentiodynamic polarization studies.
- The results were compared with surface mounting electrode using SCE.
- The results revealed that the FCME is suitable for used as an embeddable electrode for assessing the corrosion monitoring of the RC structures.

Abstract

In this study, an embeddable in-situ corrosion monitoring electrode based on Ce-doped $NiFe_2O_4$ was fabricated, and their corrosion performance of the steel rebar was evaluated in the simulated concrete environment under passive and active conditions. The passive and active environment consists of simulated concrete pore solution (SCPS) without and with 3% NaCl. The corrosion performance of embedded steel rebar in concrete was monitored by exposing the concrete specimens under alternate dry and wet condition in 3% NaCl solution. The corrosion behavior of the steel rebar was studied by using open circuit potential, AC-impedance, and potentiodynamic polarization studies. The relative corrosion performance of the embeddable steel rebar was assessed with fabricated corrosion monitoring electrode (FCME) and compared with the surface mounted electrode (SME) by using saturated calomel electrode (SCE). The results revealed that the FCME could use as an in-situ electrode for assessing the corrosion monitoring of the reinforced concrete structures.

Keywords: Embeddable electrode, surface mounted electrode, concrete pore solution, corrosion monitoring, electrochemical behavior.

1. Introduction

Reinforced concrete is protected by a thin passive film formed on the surface of the steel rebar. The high alkaline environment of the concrete pore solution enables the formation of the protective oxide film on the steel rebar surface which delays the initiation of corrosion [1]. However, the passive films get disrupted due to the ingress of chloride ions and initiate the corrosion of the embedded steel rebar with prolonged time of exposure [2]. Reinforced concrete structures, when exposed to severe marine environments, leads to the premature failure of the concrete structures [3,4]. Premature failure of the structures is minimized, and the durability of the concrete structures are enhanced by the continuous and periodical health monitoring of the concrete structures [5,6]. Health monitoring techniques include, destructive (core drilling and chloride extraction) and nondestructive techniques [7-14], electrochemical methods such as electrochemical impedance, electrochemical noise, galvanostatic pulse, linear polarization resistance, half-cell potential measurements and embeddable corrosion monitoring sensors [15-21] have been widely used to measure the corrosion of the reinforcing steel rebars in concrete. Among these methods, embeddable solid-state sensors are the most reliable technique and simply adaptable method which would be used in the field conditions

for measuring the corrosion status of the steel rebar [22]. Studies revealed that solid state sensors could able to provide more reliable and accurate status of the steel rebars (active or passive) due to the minimized IR drop, maintenance free and can be used for long-term corrosion monitoring application of reinforced concrete structures [23-28]. The in-situ durability parameters such as corrosion rate, resistivity, temperature, crack, deformation humidity, pH of the important concrete structures, bridges and other infrastructures which are located very close to the marine environments could monitor through embeddable sensors. Based on the complete information on the condition of the structure, effective control measures may be taken in advance, and the stability of the structure can be maintained [29-37]. The Ti and Ag/AgCl electrode have been used for pH and Cl^- ion concentration monitoring in concrete [38-41]. Surface mounted glass electrodes are not suitable for in-situ measurements [39] because the high resistance of the cover concrete and the dryness of the concrete will affect the conductivity of the measurements and will not able to provide the accurate results when embedded in the concrete [42]. So far, the studies have focused on MnO_2, [22-27] $NiFe_2O_4$ solid-state electrodes [28,42] for corrosion monitoring of the concrete structures. However, the long-term stability of the embedded sensor in concrete is essential for corrosion monitoring applications [43]. Nickel ferrite solid-state electrodes showed a good stability and reproducibility in chloride contaminated concrete [28,42]. Recently the development and application of nanomaterials play a vital role in the construction industries. Due to the modernization and developments in science and technology, there are a lot of advancements taking place day by day in the modern world. Likewise, construction sectors also in need of advancement and implementation of technologies in the construction practices, execution procedures, and corrosion monitoring techniques, etc. In that sense, a newer nanomaterial-based sensor was developed, and it was tried as a corrosion monitoring electrode in reinforced concrete.

In the previous part of this study [44], Ce-doped $NiFe_2O_4$ ($NiCe_{0.5}Fe_{1.5}O_4$) was developed as a novel solid-state reference electrode (SSRE) and the reversibility, electrochemical stability behavior of the electrode was studied in a buffer solution as well as synthetic concrete pore solution with and without 3.0 wt.% NaCl addition. It was found that the SSRE showed an excellent stability and reversibility in the highly alkaline environment. As an extension of the previous study, the present study aimed at evaluating the steel rebar corrosion monitored by using the fabricated corrosion rate monitoring electrode (FCME) in synthetic concrete pore solution (SCPS) under passive and active conditions (3% NaCl).

FCME was embedded in reinforced concrete specimens to monitor the corrosion of steel rebar exposed to the chloride environment under alternate wet and dry conditions. The corrosion performance of the embedded steel rebar was evaluated through electrochemical measurements such as open circuit potential, potentiodynamic polarization and electrochemical impedance spectroscopy with respect to FCME and the results are compared with the surface mounting technique.

2. Experimental Details

2.1. Materials and methods

The schematic diagram of FCME is shown in Fig. 1. The FCME assembly consists of $NiCe_{0.5}Fe_{1.5}O_4$-SSRE stainless steel 316L acted as a reference and counter electrodes respectively. The relative performance of the FCME was compared with the surface mounted electrode (SME) by using various electrochemical techniques. The SME consists of a stainless-steel sheet, in which saturated calomel electrode (SCE) is centrally embedded in the PVC sheet [45]. The SME is placed over the concrete with a sponge in between the concrete and the electrode while making the measurement the sponge was wetted with conducting gel to maintain the continuity between the embedded steel rebar and the SME.

2.2. Studies in Simulated Concrete Environment

2.2.1. Preparation of SCPS

The corrosion rate of the thermo-mechanically-treated (TMT) steel rebar was monitored in synthetic concrete pore solution (SCPS) by using FCME. The SCPS consists of 7.4 g sodium hydroxide (NaOH) and 36.6 g potassium hydroxide (KOH) per liter of saturated calcium hydroxide solution. The pH of the solution was measured using a standard portable ISTEK pH meter (Model 76P) with a relative accuracy of ± 0.001. The pH of the SCPS is 13.5.

2.2.2. Corrosion monitoring of TMT steel rebar in SCPS

In this study, 12mm dia. and 50mm length of the steel rebar was used for corrosion monitoring in SCPS with respect to FCME and SCE. The nominal composition of the TMT steel rebar used was (wt. %): 98.632% Fe, 0.193% C, 0.540% Mn, 0.281% Si, 0.024% P, 0.080% S, 0.125% Cu and 0.125% Cr. One set of steel rebars were immersed in SCPS without NaCl (passive), and another set in 3% NaCl chloride contaminated SCPS (active) for

the exposure period of 180 days. The electrochemical studies such as open circuit potential of the steel rebar, potentiodynamic polarization, and AC-impedance measurements were carried out in active and passive conditions using FCME and compared with SCE, for the exposure period of 180 days.

2.3. Electrochemical studies for rebar immersed in simulated concrete pore solution

2.3.1 Open circuit potential (OCP) measurement

The OCP measurement is an electrochemical method for monitoring the corrosion potential of the steel rebar by using high impedance voltmeter. The OCP of the steel rebar in SCPS and chloride contaminated SCPS with respect to FCME was periodically measured and for comparison purpose, the potential of the steel rebar was measured with SCE. The measurements were done as per the ASTM C876 -15 to monitor the corrosion status of the steel rebar [46].

2.3.2. Potentiodynamic polarization studies

Potentiodynamic polarization studies of the steel rebar immersed in SCPS and chloride contaminated SCPS were carried out for the exposure period of 1, 60, 120, and 180 days by considering FCME as a reference electrode. Stainless steel (SS) was used as the counter electrode and 12 mm dia. with 50 mm length of the steel rebar was used as a working electrode. During the measurement, the test solution was continuously stirred using a magnetic stirrer to avoid the concentration polarization. A time interval of 30 min. was given for each of the systems to attain a steady state condition and the OCP was noted. The potentiodynamic polarization condition corresponds to a potential sweep rate of 6 mV/min and potential ranges of −200 mV to +200 mV from the OCP. Both the anodic and cathodic polarization curves were recorded using VersaSTAT (Princeton Applied Research, Oak Ridge, TN, USA) potentiostat and the data analysis was carried out by Metrohm Autolab Nova 1.10 software by fitting the experimental data in Tafel regions. All the experiments were carried out at 30°C ± 2°C. For comparison purpose, the same experiment was carried out by using SCE as a reference electrode instead of FCME. Corrosion rate was obtained from I_{corr} and the slope of polarization curve was obtained by using the relation mentioned elsewhere [47]

$$I_{corr} = \frac{b_a b_c}{2.303(b_a + b_c)R_p}$$

$$Corrosion\ rate\ (mmpy) = 3.2 \times I_{corr}\ (\text{mA}.cm^{-2}) \times \frac{E}{D}$$

where,

b_a and b_c are anodic and cathodic slope value of Tafel plot

R_p is the polarization resistance

I_{corr} is the corrosion current density (mA.cm^{-2})

E is the equivalent weight of the steel rebar

D is the density of the steel rebar

mmpy is millimeter per year

2.3.3. AC-Impedance measurements

The same electrochemical experimental setup mentioned above was used for this study. The AC impedance studies were carried out by changing the frequency of 10 mV sinusoidal voltage from 30 kHz to 0.01 Hz. The potentiostat used was VersaSTAT (Princeton Applied Research, Oak Ridge, TN, USA) and the data analysis was carried out using Metrohm Autolab Nova 1.10 software (Ionenstrasse, Herisau, Switzerland) by fitting the experimental data in the constant phase element (CPE) model. All the experiments were carried out at 30°C ± 2°C. For comparison purpose, the same experiment was conducted for SCE. Corrosion current density was estimated from Rct values using the following expressions [48].

$$I_{corr} = {}^{B}/_{R_{ct}}$$

where,

B is the Stern Geary constant (26 mV)

R_{ct} is the charge transfer resistance of the steel rebar

2.4. Studies in Concrete - Preparation of concrete specimens

2.4.1. Materials used

Ordinary Portland Cement (OPC) of Type 1 (KS: L 5201-1989) with specific gravity 3.16 was used. The chemical composition of OPC used is given in Table 1. Fine and coarse aggregates conforming to KS: F 2526:2002 was used. Fine aggregates, passing through 2.36

mm sieve, falling under zone III with a specific gravity of 2.60 was used. Coarse aggregates consisting of crushed angular aggregates of size 10 mm and downgraded with a specific gravity 2.62 was used. The fine and coarse aggregates are washed in distilled water, dried and used for the study.

2.4.2. Casting of concrete specimen

Cylindrical concrete specimens of size 100 mm dia. and 200 mm length were cast with 12 mm diameter, 150 mm length of TMT steel rebar centrally embedded into the concrete. The FCME was embedded very near to the steel rebar. The specimens were cast using 1:1.56:3.36 mix [cement: 372 kg/m^3; sand: 580 kg/m^3; coarse aggregates: 1245 kg/m^3 with w/c ratio of 0.55]. During casting the moulds were mechanically vibrated to get a uniform surface finish along with homogenous packing of the concrete. After 24 hours, the specimens were demoulded and cured in distilled water for 28 days to avoid any contamination. The top and bottom surface of the concrete specimens were sealed with epoxy to avoid the non-uniform penetration of the chloride ions. Then the concrete specimens were subjected to alternate dry and wet cycles. Alternate dry and wet cycles were performed to accelerate the corrosion process of embedded steel rebar. One cycle consists of 3 days drying at 40°C±2°C temperature and 3 days wetting in 3% NaCl solution at 25°C±2°C. After wetting cycles, the specimens were taken out and dried at 40°C±2°C for 2 hours, and then the electrochemical measurements were carried out with respect to FCME and SME for the exposure periods of 1st, 10th, 20th and 30th cycles. The surface area of the rebar was taken for current density calculations.

2.5. Electrochemical studies for rebar embedded in concrete

2.5.1. Open circuit potential (OCP) measurement

The OCP of the steel rebar was periodically monitored with respect to FCME over the exposure period of 30 complete cycles, and the results are compared with respect to SME. The experimental procedure was described in the section 2.3.1.

2.5.2. Potentiodynamic polarization study

Potentiodynamic polarization study of the steel rebar embedded in concrete was carried out after the exposure periods of 1st, 10th, 20th and 30th cycles. The FCME was served as a reference electrode. A rectangular stainless steel and embedded steel rebar were used as

the counter and working electrodes respectively. A time interval of 30 min. was given for each of the systems to attain a steady state and the OCP was noted. The same experimental conditions as mentioned in Section 2.3.2 was followed here. For comparison purpose, the same experiment was run by using SME. In SME used system the IR compensation was done by using customized sweep mode with IR compensated value of 1Ω cm^2 [22]. The schematic diagram of the experimental setup for reinforced concrete specimen embedded with SME and FCME is shown in Fig. 2a and Fig.2b respectively.

2.5.3. AC-Impedance measurement

The reinforced concrete specimens embedded with FCME were subjected to AC-Impedance measurements in which the same experimental conditions mentioned in section 2.3.3 were followed here. For comparison, the same experiment was carried out by using SME.

3. Results and Discussion

3.1. Steel rebar corrosion monitoring in SCPS with respect to FCME and SCE

3.1.1. OCP Measurement

Fig. 3 shows the corrosion status of the steel rebar in SCPS and chloride contaminated SCPS by measuring the OCP with respect to FCME and SCE. Fig. 3a shows the OCP of the steel rebar in SCPS and chloride contaminated SCPS with respect to FCME over an exposure period of 180 days. From the figure, it is observed that the OCP of the steel rebar was -40 mV with respect FCME during the 1^{st} day of immersion in SCPS. After that, the potential was suddenly increased to +20 mV. Subsequently, the potential was gradually increased in the positive direction, and it reached +80 mV at the end of 180 days. It may be due to the passive film formation on the surface of the steel rebar in the alkaline (OH^-) environment [49-51]. The results indicated that the steel rebar was under passive state throughout the exposure period of 180 days in SCPS medium.

Further, the steel rebar immersed in chloride contaminated SCPS showed an OCP of +80 mV with respect to FCME during the 1^{st} day of exposure. After that the OCP was gradually decreased in the negative direction up to 60 days. Then, there is a sudden drop in OCP observed from 60 days to 120 days. The sudden drop in OCP may be due to the corrosion of the steel rebar/solution interface at a faster rate. After 120 days, the potential gets decreased slowly, which indicates that the speed of the corrosion reaction was slow. This may

be due to the formation of corrosion product on the steel rebar surface which blocked the entry of diffusion of corrosive ions and reduced the corrosion reaction at the steel rebar/solution interface [52]. Although, corrosion products at alkaline conditions could indeed decrease the corrosion rate; they also induce the generation of mechanical stresses at the rebar/cement interface at a slower rate.

Fig.3b shows the OCP of the steel rebar in SCPS and chloride contaminated SCPS with respect to SCE over an exposure period of 180 days. The same trend as above was observed here also. However, the steel rebar potential in SCPS with respect to SCE was -253 mV, -196 mV, -176 mV, and -136 mV during the 1st, 60, 120 and 180 days of exposure respectively. The steel rebar potential in SCPS with respect to FCME was -40 mV, +30 mV, +50 mV and +80 mV during the 1st, 60, 120 and 180 days of exposure which shows that the steel rebar is found to be under highly passive state indicating the corrosion resistance behavior [46]. At the same time when comparing the OCP of the steel rebar with respect to FCME and SCE there is some potential difference (-216 mV± 10 mV) seemed in SCPS and chloride contaminated SCPS in all exposure periods of 1st, 60, 120 and 180 days. For example, after 180 days, the OCP of the steel rebar in SCPS is relatively around +80 mV with respect to FCME and -136 mV with respect to SCE. The difference in HCP value of the steel rebar with respect to FCME and SCE was -216mV, (-136mV – (+80mV)) which is due to the stable potential of FCME (-223 ± 10 mV) [44] with respect to SCE. In addition, corrosion potential of the steel rebars with respect FCME and SCE as compared with ASTM C 876 -15 standards are given in Table 2. According to this table, the FCME is capable to determine the corrosion status of the steel rebar from the OCP measurements.

3.1.2. Potentiodynamic polarization studies

The corrosion status of the steel rebar was monitored by potentiodynamic polarization experiments in SCPS, chloride contaminated SCPS and illustrated in Fig. 4 for the exposure period of 1st, 60, 120 and 180 days. The corrosion kinetic parameters of the steel rebar immersed in SCPS and chloride contaminated SCPS were extracted after curve fitting the potentiodynamic plots in Tafel regions and the data are presented in Table 3. The steel rebar immersed in SCPS has shown the E_{corr} values of -27.69 mV, +33.75 mV, +51.14 mV and +76.25 mV with respect to FCME (Fig. 4a) and -248 mV, -193 mV, -161 mV and -145 mV (Fig. 4b) with respect to SCE respectively. I_{corr} values of the steel rebars were gradually decreased with increase in the immersion time (1st, 60, 120 and 180 days) in SCPS with

respect to FCME and SCE. These results confirmed that the potential of the steel rebar was shifted towards the passive state in SCPS under the continuous exposure to the highly alkaline medium. This is due to the formation of a thin layer of passive film on the surface of the steel rebar [53,54].

On the other hand, the potentiodynamic polarization of the steel rebar immersed in chloride contaminated SCPS for the exposure period of 1st, 60, 120 and 180 days are shown in Fig. 4c and Fig. 4d with respect FCME and SCE respectively. The corrosion kinetics parameters are calculated after curve fitting the potentiodynamic plots in Tafel regions, and the data are presented in Table 4. The E_{corr} and I_{corr} values of the steel rebar with respect to FCME and SCE were gradually shifted towards the active region in the chloride contaminated SCPS for the exposure periods from the 1st day to 180 days. For example, initially (after a day of immersion) the E_{corr} and I_{corr} values of the steel rebar were found to be -228 mV and 3.706 $\times 10^{-2}$ mA.cm^{-2} with respect to FCME and -441 mV and 3.070 $\times$ 10^{-2} mA.cm^{-2} with respect to SCE. At the end of the exposure period of 180 days, the E_{corr} and I_{corr} values of the steel rebar was found to be -355 mV and 14.031 $\times$ 10^{-2} mA.cm^{-2} with respect to FCME and -576 mV and 13.349 $\times$ 10^{-2} mA.cm^{-2} with respect to SCE. These results confirmed that FCME could able to identify the corrosion status of the steel rebar, whether it is in passive or active condition and found that the results are comparable with those of SCE. Hence, it is inferred that the FCME is suitable for use as an in-situ embeddable electrode for corrosion monitoring application in civil infrastructures.

3.1.3. AC-Impedance measurements

Fig.5a and 5b show the Nyquist plot for the steel rebar in SCPS with respect to FCME and SCE over the exposure period of 180 days. The parameters obtained from impedance measurement for various exposure periods are given in Table 5. The corrosion kinetic parameters were analyzed through the equivalent circuit (EC) model shown in Fig.5c. In the equivalent circuit model, R_s stands for the solution resistance of SCPS, R_{fp} is the resistance of the passive film, and CPE_{fp} is the constant phase element of the surface passive film, R_{ct} is the charge transfer resistance and CPE_{dl} the constant phase element double layer of the steel rebar/SCPS interface. From the Table, it is found that the resistance of the passive film (R_{fp}) increases with the increase in the exposure period. CPE_{fp} value at the first day was 2.272 $\times 10^{-3}$ $\Omega^{-1}\cdot cm^{-2}s^{-n}$ and at the 60th, 120th and 180th days were 1.179 $\times$ 10^{-3} $\Omega^{-1}\cdot cm^{-2}s^{-n}$, 1.154 $\times$ 10^{-3} $\Omega^{-1}\cdot cm^{-2}s^{-n}$ and 1.095 $\times$ 10^{-3} $\Omega^{-1}\cdot cm^{-2}s^{-n}$ respectively with respect to SCE.

Fig. 5a depicts the Nyquist plot of the steel rebar immersed in SCPS with respect to FCME. Fig.5a indicates that during the 1st day of immersion in SCPS the steel rebar is showing the passive behavior due to the film formation on the steel rebar surface in the presence of OH^- ions on the steel rebar/SCPS interface [54]. A constant pH was maintained throughout the exposure period to maintain the stable environment. After 60, 120, and 180 days, the R_{fp} and R_{ct} values were increased when compared to the initial exposure time of 1day. It may be due to the increasing adherence properties or formation of a passive film on the steel surface. The nature of the prevailing OH^- ions present in the SCPS has some impact on the corrosion resistance behavior of the steel rebar [55]. It is also observed that higher resistance and lower capacitance values indicate the passive behavior of the system [56].

Fig 5b represents the AC impedance behavior of the steel rebar immersed in SCPS with respect to SCE. The same trend as above was observed here also. It is found that as the immersion time increases, the R_{ct} value also increases revealing an enhancement of the passive film behaviour on the surface of the steel rebar [57].

Fig. 6a and Table 6 shows the impedance behavior of the steel rebar immersed in chloride contaminated SCPS with respect to FCME. From the Table, it is found that the solution resistance (R_s) was increased due to the presence of the chloride ions in SCPS. In the equivalent circuit model (Fig 7a), R_{ct}, CPE_{dl} and Z_w represent the charge transfer resistance, constant phase element of the steel rebar and Warburg diffusion of corrosive ions. In this case, passive film resistance (R_{fp}) and constant phase element (CPE_{fp}) was not obtained; this may be due to the presence of chloride ions which prevented the formation of the passive film on the steel surface [58].

After 60 days, the R_{ct} value was decreased when compared to the initial exposure time of 1 day. It indicates that the steel rebar is in the active state and aggressive ions exist in the surroundings initiated the corrosion of the steel rebar surface (Fig. 7b). Further increasing the exposure period to 120 days, the R_{ct} value was decreased when compared to 60 days. Besides in this impedance model, the R_{cp} and CPE_{cp} were obtained and is shown in Fig 7c. This may be due to the formation of a thin rust layer on the steel rebar surface. In the impedance model, R_{ct} and CPE_{dl} were the charge transfer resistance and constant phase element of the steel rebar. At 120th day the R_{cp} and CPE_{cp} values were 0.156 $k\Omega.cm^2$, 5.910 $\times 10^{-3}$ $\Omega^{-1} \cdot cm^{-2} s^{-n}$ respectively. After 180 days, the R_{cp} and R_{ct} values are slightly increased (0.207 $k\Omega.cm^2$ and 0.248 $k\Omega.cm^2$ respectively) when compared to 120 days. It may be due to the increasing thickness of the rust layer formation (Fig.7d) and it reduced the rate of

corrosion reaction on the steel rebar surface. In the meantime, Z_w also slightly decrease after 180 days when compared with 120 days. It indicates that the rate of diffusion of aggressive ions was decreased due to the further thickening of the rust layer (corrosion product) on the steel rebar surface [58,59] as shown in Fig. 7d. However, the formation of corrosion product on the steel rebar surface could not be completely controlled but the rate of corrosion reaction was reduced [60-62]. At the same time, the similar trend as above was obtained with respect to SCE (Fig. 6b).

Fig. 8 shows the impedance modulus and phase angle plots of the steel rebar in SCPS with respect to FCME and SCE for the exposure period of 180 days. The impedance modulus plot reveals that; the high-frequency impedance corresponds to the solution resistance (R_s). The low-frequency impedance corresponds to the total impedance equals to the solution resistance (R_s), passive film resistance (R_{fp}), corrosion product resistance (R_{cp}) and the charge transfer resistance (R_{ct}) and it also includes the capacitance (CPE_{fp}, CPE_{cp} and CPE_{ct}) [63]. Fig. 8a shows that under low-frequency the impedance values were gradually increased in SCPS at the increasing exposure period of 60, 120 and 180 days. This may be due to the formation of the passive film on the steel rebar surface [53,54]. This indicates the improvement in corrosion resistance properties of the steel rebar in SCPS with respect to FCME.

Fig. 8b shows the phase angle plot of the steel rebar immersed in SCPS with respect to FCME. From the figure, it is found that a highly capacitive behavior is observed in the medium to low- frequency range of 10^{2}-10^{-1} Hz, which is due to the formation of the passive film on the steel rebar surface. Assis and Costa et al. [64] reported that the broad capacitive phase angle in the medium frequency region is due to the outer porous layer whereas the one at lower frequencies, to the inner barrier layer of the steel rebar surface. This type of behavior indicates that a highly stable protecting film [64,65] is formed on the surface of the steel rebar with increasing immersion time until the end of 180 days. Whereas under medium to low-frequency range the phase angle values were increasing with the exposure period of 1, 60, 120 and 180 days. The phase angles close to - 75° (180 days) from medium to low-frequency indicates that the oxide film formed is highly protective. Impedance modulus and phase angle diagrams concluded that the steel rebar continuously immersed in SCPS at constant pH protected the steel rebar against corrosion, due to the thickening of the passive film with increasing immersion time [64]. The same type of behavior was observed for SCPS with respect to SCE (Fig. 8c-d). Fig. 9 shows the impedance modulus and phase angle plots of the

steel rebar in chloride contaminated SCPS with respect to FCME and SCE for the exposure period of 1st, 60, 120 and 180 days. Fig. 9a shows the impedance modulus plot in which the impedance value decreases with increasing the immersion time up to 120 days; this indicates that the decrease in the stability and corrosion resistance behavior of the steel rebar. But with the increasing immersion period to 180 days, the impedance values were slightly increased which is mainly attributed to the corrosion product formed on the steel rebar surface [66]. This type of corrosion product slightly reduced the rate of the corrosion reaction of the steel rebar.

The phase angle plot is shown in Fig. 9b. The phase angle values decrease with the increasing immersion time. During the 1st and 60th days of exposure, the steel rebar is showing the capacitive behavior in the medium frequency range 10^2 to 10^0. Further with the increasing immersion time to 120 and 180 days the peak value of the phase angle also decreases and the capacitive behavior is shifted to the medium frequency range of 10^2 to 10^1. While the reduction of peak height [67] with increasing exposure time indicating the decay of the capacitive impedance of the surface film causing corrosion. Besides, at 120 and 180 days of exposure period the phase angle of the steel rebar, was suddenly increased and decreased again and makes the capacitive behavior in the region of 10^0 to 10^{-1}. Which may be attributed to the more corrosion product formed on the steel rebar surface [68,69].

On the other hand, the impedance modulus and phase angle plots of the steel rebar embedded in SCPS and chloride contaminated SCPS with respect to SCE are given in Fig 8c-d and Fig. 9c-d. The same trend was observed for the steel rebar immersed in chloride contaminated SCPS with respect to SCE. These results confirmed that FCME is having the ability to differentiate between the active and passive condition of the steel rebar. Therefore, from the above results, it is inferred that FCME could use as an in-situ embeddable corrosion monitoring electrode for reinforced concrete structures.

3.2. Corrosion monitoring in concrete

3.2.1. OCP measurements

Fig. 10 shows the OCP of the steel rebar embedded in concrete with respect to FCME and SME for the steel rebar embedded in concrete at the various number of cycles. During the 1st and 10th cycle of exposure, the steel rebar has shown an OCP of -10 and -25 mV vs. FCME indicating the passive condition of the steel rebar. After the 10th cycle, there is a sudden increase in the OCP towards the more negative direction and it reaches the potential

of -52 mV vs. FCME (threshold potential of -275 mV vs. SCE) at the 12th cycle of exposure. After 12th cycle, the potential was gradually shifted towards the more negative direction indicating the chloride ions reached the rebar level at a faster rate and induced the corrosion of the steel rebar. From 20th cycle until the end of the 30th cycle the potential decreases at a lower rate indicating that the corrosion reaction is occurring slowly. On the other hand, more fluctuation in OCP measurement is observed up to 10th cycle with respect to SME. This fluctuation in the OCP may be related to the unstable conductive path due to the absence of the moisture content in the inner parts of the concrete. After the 10th cycle of exposure, the potential value was decreased faster than the previous cycles due to the consequence of the chloride attack which initiated the corrosion of the rebar and the potential fluctuation was gradually decreased due to the penetration of the chloride ions which increased the conductivity between the steel rebar and SME.

This type of potential fluctuation does not appear with respect to FCME. Because the FCME is embedded very near (10 mm) to the steel rebar this significantly reduced the IR drop and displayed a more stable OCP. Further, it is concluded that FCME could able to predict the status of the steel rebar whether it is in a passive or active state.

3.2.2. Potentiodynamic Polarization

The potentiodynamic polarization curves for embedded steel rebar in the concrete medium are shown in Fig. 11 with respect FCME (Fig.11a) and SME (Fig. 11b) for the exposure period of 180 days. The corrosion kinetics parameters of the steel rebar embedded in concrete are given in Table 7. During the 1st and 10th cycle, the E_{corr} and I_{corr} values of the steel rebar in concrete was -12.89 mV, 0.206 × 10^{-2} mA.cm^{-2} and -28.34 mV, 0.268 × 10^{-2} mA.cm^{-2} with respect to FCME. There is no significant change seen up to 10th cycles, i.e. the difference in E_{corr} values between the 1st and 10th cycle was observed as +15.45 mV. These results confirmed that the corrosion reactions occurring in the embedded steel rebar were very slow. It is due to the existence of the insufficient amount of chloride ions surrounding the steel rebar and complex salt formation of Friedel's salt which reduced the pores [70,71] in concrete up to the 10th cycle. After the 20th cycle, the E_{corr} and I_{corr} values of the embedded steel rebar were -165.79 mV and 1.44 × 10^{-2} mA.cm^{-2} with respect to FCME. Comparing the 10th and 20th cycles, the difference in E_{corr} value is +137.45 mV vs. FCME. These observations indicated that the steel rebar is corroding at a faster rate due to the penetration of free chloride ions which reached the surface of the steel rebar. After 30th cycle, the E_{corr} and

I_{corr} values were further increased (-218 mV and 2.744 × 10^{-2} mA/cm^{-2}) due to the continuous ingress of chloride ions indicating the severe corrosive nature of the steel rebar. Comparing the 20th and 30th cycles, the difference in E_{corr} value is +52.21 mV vs. SME. These results confirmed that rate of corrosion reaction was reduced at the 30th cycle. It may be due to the formation of corrosion product on the steel rebar surface which controlled the diffusion of aggressive ions [72]. Potentiodynamic polarization curve for embedded steel rebar with respect SME is shown in Fig. 11b. In this case, also similar observation was noticed. However, during the initial period of exposure (1st and 10th cycles) some potential fluctuation has appeared in potentiodynamic polarization plot. Therefore, the conductivity between the steel rebar and SME was decreased, which led to the potential fluctuation. This fluctuation was gradually decreased over the continuous exposure of 20th and 30th cycles. The reason is that the diffused chloride ions increased the conductivity between the steel rebar and SME. This type of potential fluctuation was overcome by using the FCME. Because the FCME was embedded very near to the steel rebar which minimized the IR drop between the electrode and the steel rebar embedded in concrete.

3.2.3. AC-Impedance measurement

Fig. 12 shows the AC impedance curve for the steel rebar embedded in concrete with respect to FCME and SME at a various number of cycles. Fig.13 shows the AC impedance equivalent circuit model and schematic diagram of the steel rebar in concrete over the exposure period of 180 days. The parameters obtained from the impedance plot for the steel rebar embedded in concrete with respect to FCME and SME are shown in Table 8. In this table, R_s stands for the solution or moisture resistance, R_{cr} the resistance of the concrete between the working electrode and the reference electrode, CPE_{cr} the constant phase element of the concrete between the working and reference electrode. R_{fp} resistance of the surface passive film, CPE_{fp} the constant phase element of the surface passive film, R_{cp} the resistance of corrosion products on the steel rebar surface, CPE_{cp} constant phase elements of corrosion products on the steel rebar surface, R_{ct} the charge transfer resistance of the steel rebar and CPE_{dl} the constant phase element of the steel rebar. Fig.12a is showing the resistive behavior of the steel rebar with respect to FCME during the 1st and 10th cycles of the exposure indicating the passive nature of the steel rebar. From Table 8 it is found that R_s and R_{cr} values were found to decrease with the increase in an exposure period with respect to FCME. It may be due to the diffused chloride ions which increased the conductivity of the concrete. The

CPE_{cr} value of the embedded steel rebar was also increased during the 1st, 10th, 20th and 30th cycles were 0.163 × 10^{-7}, 0.182 × 10^{-7}, 1.24 × 10^{-7}, and 41.83 × 10^{-7} respectively for FCME. During the 1st cycle of exposure, the passive film resistance (R_{fp}) and the charge transfer resistance R_{ct} of the steel rebar was found to be 0.439 kΩ.cm^2 and 1.95 kΩ.cm^2 respectively indicating the passive behavior of the steel rebar. During the 10th cycle, R_{fp} and R_{ct} were decreased to 0.269 kΩ.cm^2 and 1.324 kΩ.cm^2. The decrease in R_{fp} and R_{ct} value at the 10th cycle were 1.63 and 1.47 times lesser than that of the 1st cycle. The slow decrease in the R_{fp} and R_{ct} value may be due to the complex formation which reduced the pores and slow ingress of chloride ions [70], slowly begins to destroy the passive film formed on the steel surface. At the 20th cycle, there is an immediate drop in the charge transfer resistance value R_{ct} (0.562 kΩ.cm^2), i.e., the decrease in R_{ct} values at the 20th cycle was 2.36 times that of the 10th cycle. This observation indicates the continuous penetration of chloride ions surrounding the concrete reached the surface of the steel rebar and destroyed the passive film and formed a thin layer of corrosion product on the steel rebar surface. Because, at this cycle, both the diffusion and charge transfer processes have accelerated the corrosion of the steel rebar [72]. The R_{ct} value was further decreased to 0.350 kΩ.cm^2 at the 30th cycle indicating the continuous process of corrosion led to the increase in the thickness of the rust layer but at a slower rate than the 20th cycle. Here, the R_{ct} value at the 30th cycle was 1.60 times lesser than that of the 20th cycle. The reason for this decrease is due to the increase in thickness of the corrosion product formation which slightly reduced the rate of corrosion reaction [58,59]. Hence, R_{cp} and CPE_{cp} value was found in the 30th cycle of exposure indicating the continuous process of corrosion taking place in the embedded steel rebar [73]. The resistance (R_{cp}) and constant phase element (CPE_{cp}) of the corrosion product values were 0.251 kΩ.cm^2 and 0.0138 $\Omega^{-1}\cdot cm^{-2}s^{-n}$ ×10^{-3} respectively at the 30th cycle of the exposure. The Z_w of the steel rebar at the 1st cycle was 0.392 ×10^{-3} $\Omega\cdot cm^2s^{0.5}$ and in the 10th cycle the values was shifted to 0.602 ×10-3 $\Omega\cdot cm^2$s0.5 and in the 20th cycle again it was increased to 2.01 ×10^{-3} $\Omega\cdot cm^2s^{0.5}$ and finally the value was slightly decreased to 1.99 ×10^{-3} $\Omega\cdot cm^2s^{0.5}$.

In the case of SME, the same trend was observed. The R_s and R_{cr} value was decreased from the 1st cycle to 30th cycle. The resistance of the concrete has been reduced due to the diffusion of chloride ions via the porous nature of concrete and increasing the conductivity between the steel rebar and SME. CPE_{dl} value was found to increase with the increase in the exposure period indicating the continuous process of corrosion taking place in the embedded steel rebar [73].

From Table 8 it is obvious that, when compared to FCME, all the values measured with SME are found to be higher indicating the higher resistance existing in the concrete which influenced the measurements. From the Fig. 12b it is observed that during the 1^{st} and 10^{th} cycle there is a huge fluctuation in the readings observed due to the high resistance and low conductivity of the concrete but at the 20^{th} and 30^{th} cycle the fluctuations are not observed due to the continuous penetration of chloride ions which increased the conductivity of the concrete.

From the results, it is inferred that FCME gave reliable results when compared to the SME. Furthermore, by using FCME the concrete resistance is minimized and the results observed are found to be satisfactory. Fig.14 shows the Impedance modulus plot and phase angle for the steel rebar embedded in concrete with respect to FCME and SME. Fig. 14a shows that under low frequency, the impedance values of the embedded steel rebar in concrete with respect to FCME was gradually decreased with the increasing exposure period of 1^{st}, 10^{th} and 20^{th} cycle indicating the corrosive condition of the steel rebar due to the gradual penetration of the chloride ions. But at the 30^{th} cycle, there is a slight increase in the impedance value observed indicating that the corrosion product formed on the steel rebar surface was acting as a barrier and further it has blocked the pores for the entry of chloride ions [66,72]. So, the impedance values were slightly increased at the 30^{th} cycle of the exposure. Fig. 14b shows the phase angle plot of the rebar embedded in concrete with respect to FCME. From the figure, it is found that a resistive behavior is observed in the larger frequency range of 10^2-10^4 Hz. Whereas under medium to low-frequency range (10^0 to 10^1) it is showing the slight capacitive behavior and the phase angle was decreasing with the exposure period. By increasing the exposure period to 20^{th} and 30^{th} cycle, the capacitive behavior is slightly shifted to the higher frequency region and the phase angle occurs a diffusion tail at low-frequency region, which indicates the mass transfer behavior occurs on the steel rebar/concrete interface [74]. This type of behavior indicates that a protecting film was disrupted and corrosion was taking place gradually due to the continuous penetration of the chloride ions.

The same type of behavior was overserved for the steel rebar embedded in concrete with respect to SME (Fig. 14c-d). However, during the 1^{st} cycle, high impedance value was attained (Fig 14c) at the high-frequency region ($10^2 – 10^4$) indicating the high resistance of concrete [75]. Herein, during the 1^{st} and 10^{th} cycle, a lot of fluctuations were observed in the impedance modulus plot and phase angle plot. The fluctuation may be due to the poor conductivity between the electrode and the embedded steel rebar. After that, the impedance

value was gradually decreased at the 10^{th}, 20^{th} and 30^{th} cycles. Hence this result also confirmed that the resistance of the concrete gradually decreases due to the penetration of chloride ions through the porous nature of the concrete, which increased the conductivity of the concrete. From the results, it is found that the embeddable electrode (FCME) performs better than the SME in the concrete environment.

3.3 Mechanism of Ce doped $NiFe_2O_4$ FCME in concrete environment

The electrochemical reaction taking place in Ce doped $NiFe_2O_4$ FCME is that the galvanic potential of the nickel ferrite originates as Ni^{2+}/Ni^{3+} redox coupling [28]. In addition, Ce doping in $NiFe_2O_4$ decreases the magnetic dipolar interaction, reduces the particle size and improves the electrochemical reversibility of $NiFe_2O_4$ [44].

4. Conclusions

The following conclusions could be drawn from the above investigation:

- The developed FCME can use as an in-situ corrosion monitoring sensor for detecting the corrosion behavior of reinforcing steel rebar in concrete.
- The FCME is a tool used to measure the corrosion potential, corrosion current and impedance behavior of the steel rebar embedded in concrete.
- Hence FCME is a promising tool for predicting the accurate information on the corrosion status of the steel rebar, whether it is in passive or active condition.
- FCME is embedded very near to the steel rebar which eliminates the IR drop between the steel rebar and electrode.
- These electrodes are suitable for long-term application in corrosion monitoring of reinforced concrete.
- Therefore, from the above results, it is inferred that FCME could use as an embeddable in-situ electrode for corrosion monitoring in the concrete structure.

Acknowledgement

This research was supported by the Basic Science Research Program through the National Research Foundation of Korea (NRF) funded by the Ministry of Science, ICT, & Future Planning (No. 2015R1A5A1037548). One of the authors (V.S) thanks the Director, CECRI, and CSIR for the permission to pursue my fellowship at Hanyang University, Korea.

References

1. N. Byrne, Holmes, B. Norton, State-of-the-art review of cathodic protection for reinforced concrete structures, Mag. Concr. Res. 68(13) (2016) 664-677.

2. P.B. Raja, S. Ghoreishiamiri, M. Ismail, Natural corrosion inhibitors for steel reinforcement in concrete – a review, Surf. Rev. Lett. 22(3) (2015) 8.

3. A. Sivasankar, S. Arul Xavier Stango, R. Vedalakshmi, Quantitative estimation on delaying of onset of corrosion of rebar in surface treated concrete using sealers, Ain Shams Eng. J. 4 (2013) 615-623.

4. X. Wang, M.G. Stewart, M. Nguyen, Impact of climate change on corrosion and damage to concrete infrastructure in Australia, Clim. Change. 110 (2012) 941-957.

5. M. Sun, W.J. Staszewski, R.N. Swamy, Smart sensing technologies for structural health monitoring of civil engineering structures – A review, Adv. Civil Eng. 2010 (2010) 1-13.

6. Jianghong Mao, Jiayun Chen, Lei Cui, Weiliang Jin, Chen Xu, Yong He, Monitoring the corrosion process of reinforced concrete using BOTDA and FBG sensors, Sensors 15 (2015) 8866-8883.

7. J. Malek, M. Kaouther, Destructive and non-destructive techniques of concrete structures, Jordan Journal of Civil Engineering, 8(4) (2014) 432-441.

8. P. Shaw, A. Xu, Assessment of the deterioration of concrete in NPP- causes effects and investigation methods, NDT. Net. 3(2) (1998).

9. D.M. McCann, M.C. Forde, Review of NDT methods in the assessment of concrete and masonry structures, NDT and E Inter. 34(2) (2001) 71-84.

10. D. Breysse, G. Klysz, X. Dérobert, C. Sirieix, J.F. Lataste, How to combine several non-destructive techniques for a better assessment of concrete structures, Cem. Concr. Res. 38(6) (2008) 783-793.

11. M. Sanayei, J.E. Phelps, J.D. Sipple, E.S. Bell, B.R. Brenner, Instrumentation, non-destructive testing, and finite element model updating for bridge evaluation using strain measurements, J. Bridge Eng. 17(1) (2012) 130-138.

12. S.K. Verma, S.S. Bhaduaria, S. Akhtar, Review of non-destructive testing for condition monitoring of concrete structures, J. Constr. Eng. 2013 (2013) 11.

13. D. Breysse, Non-destructive evaluation of concrete strength: a historical review and a new perspective by combining NDT methods, Constr. Build. Mater. 33 (2012) 139-163.

14. F. Aydin, M. Saribiyik, Correlation between Schmidt hammer and destructive compressions testing for concretes in existing buildings, Sci. Res. Essays 5 (2010) 1644-1648.

15. H.W. Song, V. Saraswathy Corrosion monitoring of reinforced concrete structures - A Review, Int. J. Electrochem. Sci. 2 (2007) 1-28.

16. R. Vedalakshmi, K. Thangavel, Reliability of Electrochemical Techniques to Predict the Corrosion Rate of Steel in Concrete Structures, Arabian J. Sci. Eng. 36 (2011) 769-783.

17. S. Sathiyanarayanan, N. Panjali, K. Saravanan, S. Srinivasan, G. Venkatachari, Corrosion monitoring of steel in concrete by galvanostatic pulse technique, Cem. Concr. Compos. 28 (2006) 630-637.

18. E. Escalante, Effectiveness of potential measurements for estimating corrosion of steel in concrete. In: Corrosion of Reinforcement in Concrete, Elsevier, London 1990, p. 281.

19. J.S. Ryu, N. Otsuki, Application of electrochemical techniques for the control of cracks and steel corrosion in concrete, J. Appl. Electrochem. 32 (2002) 635-639.

20. B. Elsener, S. Muller, M. Suter, H. Bohni, Corrosion monitoring of steel in concrete: theory and practice. In: Corrosion of Reinforcement in Concrete, Elsevier, London, 1990, p. 348.

21. N. Birbilis, B.W. Cherry, Alternative methodology for on-site monitoring of corrosion and remediation of reinforced concrete, Corros. Eng. Sci. Technol. 39 (4) (2004) 321-326.

22. S.P. Karthick, S. Muralidharan, V. Saraswathy, K. Thangavel, Long-term relative

performance of embedded sensor and surface mounted sensor for corrosion monitoring of steel in concrete structures, Sens. Actuators B: Chem. 192 (2014) 303-309.

23. T.H. Ha, S. Muralidharan, J.H. Bae, Y.C. Ha, H.G. Lee, K.W. Park, D.K. Kim, Role of sensors in corrosion monitoring and durability assessment in concrete structures: the state of the art, Sens. Mater. 16 (2004) 133-158.

24. S. Muralidharan, V. Saraswathy, A. Madhavamayandi, K. Thangavel, N. Palaniswamy, Evaluation of embeddable potential sensor for corrosion monitoring in concrete structures, Electrochim. Acta 53 (2008) 7248-7254.

25. S. Muralidharan, T.H. Ha, J.H. Bae, Y.C. Ha, H.G. Lee, K.W. Park, D.K. Kim, Electrochemical studies on the performance characteristics of solid metal–metal oxide reference sensor for concrete environments, Sens. Actuators B: Chem. 113 (2006) 187-193.

26. S. Muralidharan, T.H. Ha, J.H. Bae, Y.C. Ha, H.G. Lee, K.W. Park, D.K. Kim, Electrochemical studies on the solid embeddable reference sensors for corrosion monitoring in concrete structure, Mater. Lett. 60 (2006) 651-655.

27. S. Muralidharan, V. Saraswathy, K. Thangavel, N. Palaniswamy, Electrochemical studies on the performance characteristics of alkaline solid embeddable sensor for concrete environments, Sens. Actuators B Chem. 130 (2008) 864-870.

28. S. Muralidharan, V. Saraswathy, L. John Berchmans, K.Thangavel, Ki Yong Ann, Nickel ferrite ($NiFe_2O_4$): A possible candidate material as reference electrode for corrosion monitoring of steel in concrete environments, Sens. .Actuators B: Chem. 145 (2010) 225-231.

29. S.Y. Li, Y.G. Kim, S. Jung, H.S. Song, S.M. Lee, Application of steel thin film electrical resistance sensor for in situ corrosion monitoring, Sens. Actuators B Chem. 120 (2007) 368-377.

30. M. Blumentritt, K. Melhorn, J. Flachsbarth, M. Kroener, W. Kowalsky, H.H. Johannes, A novel fabrication method of fiber-optical planar transmission sensors for monitoring pH in concrete structures, Sens. Actuators B Chem. 131 (2008) 504-508.

31. M. Ghandehari, C.S. Vimer, In situ monitoring of pH level with fiber optic evanescent field spectroscopy, NDT&E Inter. 37 (2004) 611-616.

32. C.K.Y. Leung, Fiber optic sensors in concrete: the future? NDT & E Inter. 34 (2001) 85-94.

33. Z. Zhang, F. Ansari, Fiber-optic laser speckle-intensity crack sensor for embedment in concrete, Sens. Actuators A Phy. 126 (2006) 107-111.

34. B. Glisi, N. Simon, Monitoring of concrete at very early age using stiff SOFO sensor, Cem. Concr. Compos. 22 (2000) 115-119.

35. A. Norris, M. Saafi, P. Romine, Temperature and moisture monitoring in concrete structures using embedded nanotechnology/microelectromechanical systems (MEMS) sensors, Constr. Build. Mater. 22 (2008) 111-120.

36. M. Raupach, P. Schie, Macrocell sensor systems for monitoring of the corrosion risk of the reinforcement in concrete structures, NDT & E Inter. 34 (2001) 435-442.

37. H. Liao, J.C. Chou, Preparation and characterization of the titanium dioxide thin films used for pH electrode and procaine drug sensor by sol–gel method, Mater. Chem. Phys. 114 (2009) 542-548.

38. S.A.M. Marzouk, Improved Electrodeposited Iridium Oxide pH Sensor Fabricated on Etched Titanium Substrates, Anal. Chem. 75 (2003) 1258-1266.

39. G.D. Rong, G.H. Rong, S.H. Ruo, J.L. Chang, In situ measurement of Cl^- concentrations and pH at the reinforcing steel/concrete interface by combination sensors, Anal. Chem. 78 (2006) 3179-3185.

40. M.A. Climent-Llorca, E. Viqueira-Perez, M.M. Lopez-Atalaya, Embeddable Ag/AgCl sensors for in-situ monitoring chloride contents in concrete, Cem. Concr. Res. 26, (1996) 1157-1161.

41. C.E. Locke, C. Dehghanian, Embeddable reference electrodes for chloride contaminated concrete, Mater. Perform. 18 (1970) 70-73.

42. V. Maruthapandian, S. Muralidharan, V. Saraswathy, Spinel $NiFe_2O_4$ based solid state embeddable reference electrode for corrosion monitoring of reinforced concrete structures, Constr. Build. Mater. 107 (2016) 28-37.

43. S. Muralidharan, T.H. Ha, J.H. Bae, Y.C. Ha, H.G. Lee, D.K. Kim, A promising potential embeddable sensor for corrosion monitoring application in concrete structures, Measurement 40 (2007) 600-606.

44. Subbiah Karthick, Han Seung Lee, Yun Su Lee, Jitendra Kumar Singh, Seung-Jun Kwon, Rethinam Natarajan, Fabrication of a cerium-doped nickel ferrite solid state reference electrode and its performance evaluation in concrete environment, Sens. Actuators B Chem. 251 (2017) 509-523.

45. R. Vedalakshmi, H. Dolli, N. Palaniswamy, Embeddable corrosion rate-measuring sensor for assessing the corrosion risk of steel in concrete structures, Struct. Control Health Monit. 16 (2009) 441-459.

46. ASTM C876-15, Standard Test Method for Corrosion Potentials of Uncoated Reinforcing Steel in Concrete, ASTM International, West Conshohocken, PA, 2015.

47. ASTM G 102 – 89, Standard Practice for Calculation of Corrosion Rates and Related Information from Electrochemical Measurements, ASTM International, West Conshohocken, PA, 1999.

48. K. Ganesan, K. Rajagopal, K. Thangavel, Evaluation of bagasse ash as corrosion resisting admixture for carbon steel in concrete, Anti-Corros. Method. Mater. 54(4) (2007) 230-236.

49. M. Jayalakshmi, V.S. Muralidharan Passivation and hydrogen evolution studies on iron in alkali solutions, Corros. Rev. 12 (1994) 305-320.

50. R.S. Schrebler Guzman, J.R. Vilche, A.J. Arvia, The voltammetry detection of intermediate electrochemical processes related to iron in alkaline aqueous solutions, J. Appl. Electrochem. 11 (1981) 551-561

51. R.S. Schrebler Guzman, J.R. Vilche, A.J. Arvia, The potentiodynamic behaviour of iron in alkaline solutions, Electrochim. Acta, 24 (1979) 395-403.

52. Y. Morozov, A.S. Castela, A.P.S. Dias, M.F. Montemor, Chloride-induced corrosion behaviour of reinforcing steel in spent fluid cracking catalyst modified mortars, Cem. Concr. Res. 47 (2013) 1-7.

53. Jin-yang Jiang, Danqian Wang, Hong-yan Chu, Han Ma, Yao Liu, Yun Gao, Jinjie Shi, Wei Sun, The passive film growth mechanism of new corrosion-resistant steel rebar in simulated concrete pore solution: nanometer structure and electrochemical study, Materials 10 (2017) 412-426.

54. M. Sanchez, J. Gregori, C. Alonso, J.J. Garcia-Jareno, H. Takenouti, F. Vicente, Electrochemical impedance spectroscopy for studying passive layers on steel rebars immersed in alkaline solutions simulating concrete pores, Electrochim. Acta 52 (2007) 7634-7641.

55. L. Freire, M. Carmezim, M. Carmezim, Ma Ferreira, M. Montemor, The passive behaviour of AISI 316 in alkaline media and the effect of pH: a combined electrochemical and analytical study, Electrochim. Acta, 55 (21) (2010) 6174-618.

56. D.V. Ribeiro, C.A.C. Souza, J.C.C. Abrantes, Use of electrochemical impedance spectroscopy (EIS) to monitoring the corrosion of reinforced concrete, IBRACON Structures and Materials J. 8(4) (2015) 529-546.

57. H. Luo, C.F. Dong, X.G. Li, K. Xiao, The electrochemical behaviour of 2205 duplex stainless steel in alkaline solutions with different pH in the presence of chloride, Electrochim. Acta, 64 (2012) 211-220.

58. Hakim Bensabra, Noureddine Azzouz, Study of rust effect on the corrosion behaviour of reinforcement steel using impedance spectroscopy, Metall. Mater. Trans. A. 44(13) (2013) 5703-5710.

59. L.A. Nikfahm, I. Danaee, A. Ashrafi, M.R. Toroghinejad, Effect of grain size changes on corrosion behaviour of copper produced by accumulative roll bonding Process, Mater. Res. 16(6) (2013) 1379-1386.

60. A. Rosenberg, C.M. Hansson, C. Andrade, Mechanisms of corrosion of steel in concrete, in the materials science of concrete, J. Skalny, Editor, The American Ceramic Society, 1989, p. 285-313.

61. C. M. Hansson, Comments on electrochemical measurements of the rate of corrosion of steel in concrete, Cem. Concr. Res. 14 (1984) 547-584.

62. ACI Committee 222, 222R-96, Corrosion of Metals in Concrete, 1996.

63. A. Amirudin, D. Thierry, Application of electrochemical impedance spectroscopy to study the degradation of polymer-coated metals, Prog. Org Coat. 26 (1995) 1-28.

64. Sergio Luiz de Assis, Isolda Costa, The effect of hydrogen peroxide on the electrochemical behaviour of Ti-13Nb-13Zr alloy in Hanks solution, Mater. Res. 9(4) (2006) 425-429.

65. I.C. Lavos-Valereto, S. Wolynec, I. Ramires, A.C. Guastaldi, I. Costa, Electrochemical impedance spectroscopy characterization of passive film formed on implant Ti-6Al-7Nb alloy in Hanks' solution, J. Mater. Sci. Mater. Medicine. 15(1) (2004) 55-59.

66. H. Nady, M.M. El-Rabiei, M. Samy, Corrosion behaviour and electrochemical properties of carbon steel, commercial pure titanium, copper and copper–aluminum–nickel alloy in 3.5% sodium chloride containing sulfide ions, Egyptian J.Petroleum. 26(1) (2017) 79-94.

67. Fujian Tang, Yi Bao, Yizheng Chen, Yan Tang, Genda Chen, Impact and corrosion resistances of duplex epoxy/enamel coated plates, Constr. Build. Mater. 112 (2016) 7-18.

68. M. Curioni, F. Scenini, T. Monetta, Correlation between electrochemical impedance measurements and corrosion rate of magnesium investigated by real-time hydrogen measurement and optical imaging, Electrochim. Acta, 166 (2015) 372-384.

69. A.C. Bastos, A.M.P. Simoes, Effect of deep drawing on the performance of coil-coatings assessed by electrochemical techniques, Prog. Org. Coat. 65 (2009) 295-303.

70. R. Vedalakshmi, R. Renugha Devi, B. Emmanuel, N. Palaniswamy, Determination of diffusion coefficient of chloride in concrete: an electrochemical impedance spectroscopic approach, Mater. Struct. 41(7) (2008) 1315-1326.

71. S.P. Karthick, S. Muralidharan, V. Saraswathy, S-J. Kwon, Effect of different alkali salt additions on concrete durability property, J. Struct. Integ. Mainten. 1 (2016) 35-42.

72. J. Wei, J.H. Dong, W. Ke, Corrosion evolution of scaled rebar in concrete under dry/wet cyclic condition in 3.5% NaCl solution, Int. J. Electrochem. Sci. 8 (2013) 2536-2550.

73. C. Liu, Q. Bi, A. Leyland, A. Matthews, An electrochemical impedance spectroscopy study of the corrosion behaviour of PVD coated steels in 0.5 N NaCl aqueous solution: Part II.: EIS interpretation of corrosion behavior, Corros. Sci. 45 (2003) 1257-1273.

74. J. Flis, H. W. Pickering, K. Osseo-Asare, Interpretation of impedance data for reinforcing steel in alkaline solution containing chlorides and acetates, Electrochim. Acta. 43 (1998) 1921-1929.

75. KangkangTang, Stray current induced corrosion of steel fibre reinforced concrete, Cem. Concr. Res. 100 (2017) 445-456.

List of Figures

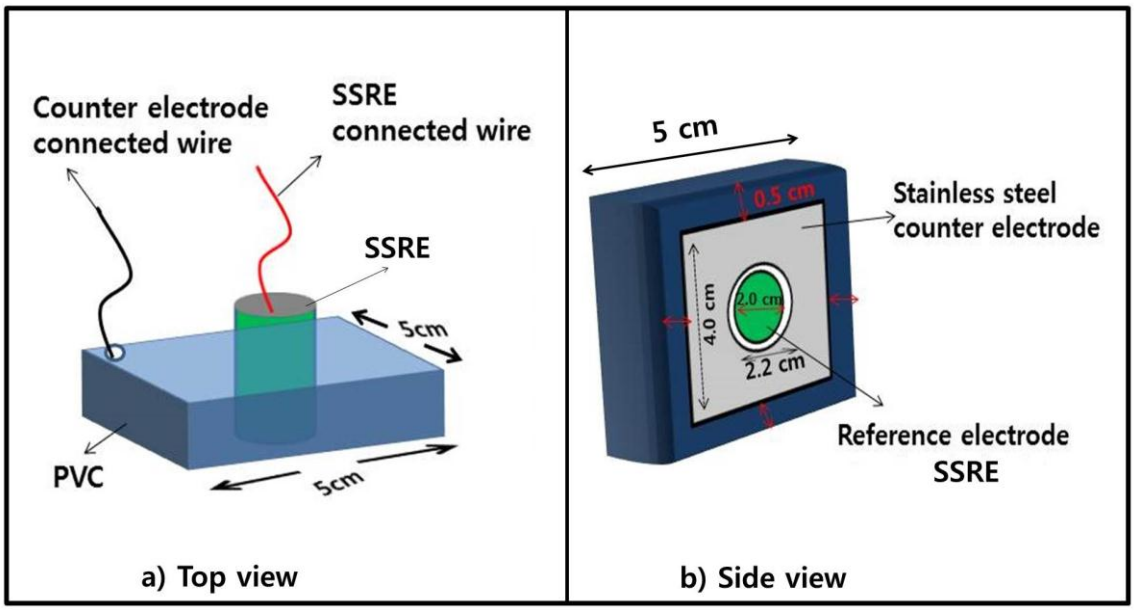

Fig. 1. Schematic diagram of FCME

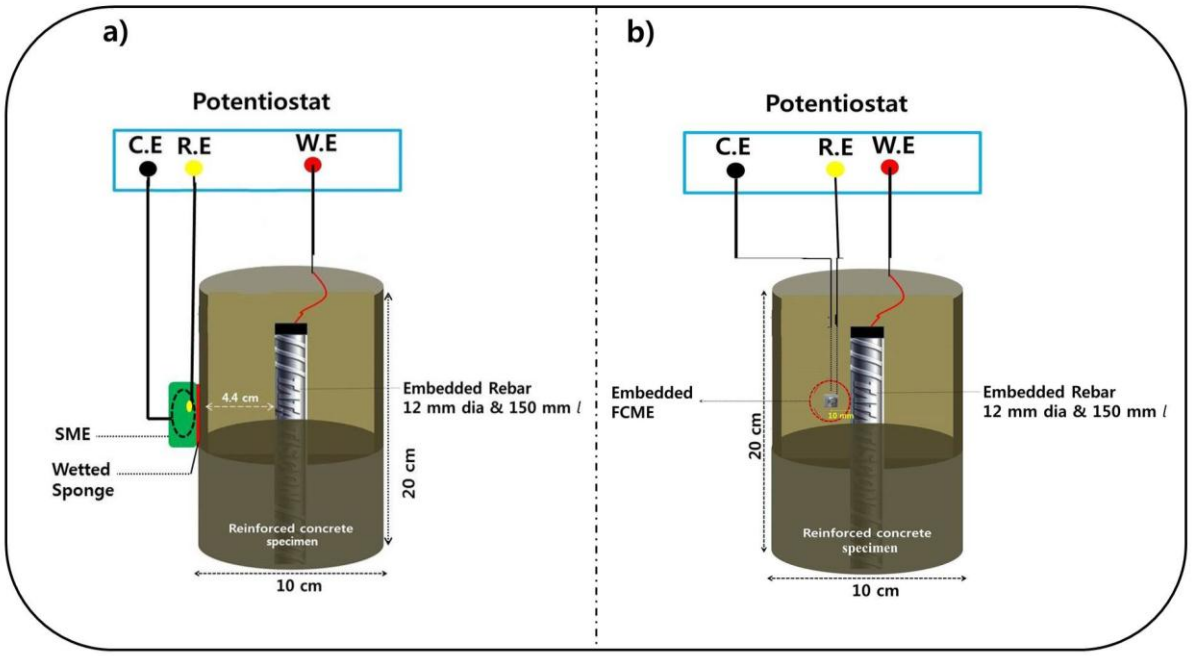

Fig. 2. Schematic diagram of experimental setup for reinforced concrete specimen with respect SME (a) and FCME (b)

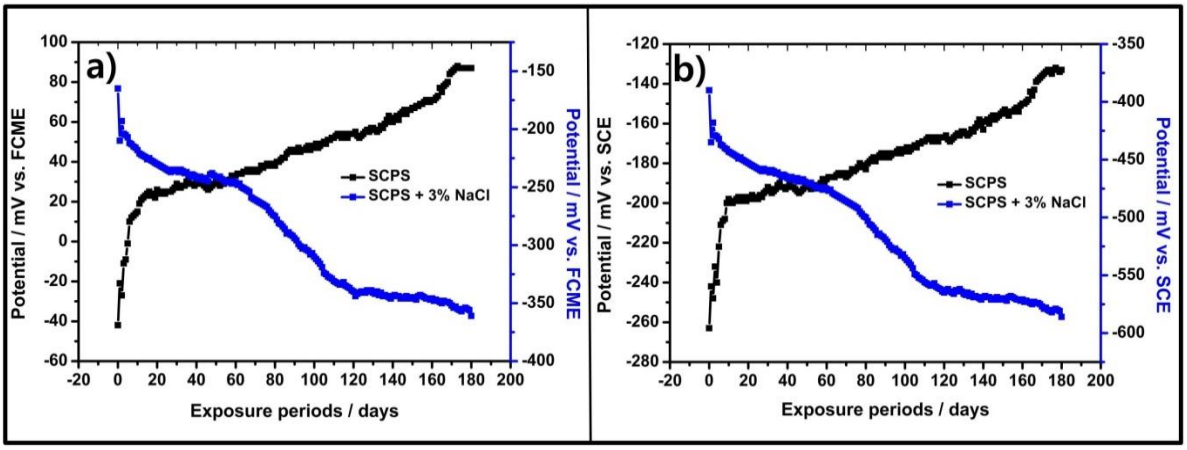

Fig. 3. The OCP of the steel rebar immersion SCPS and chloride contaminated SCPS with respect to FCME (a); SCE(b).

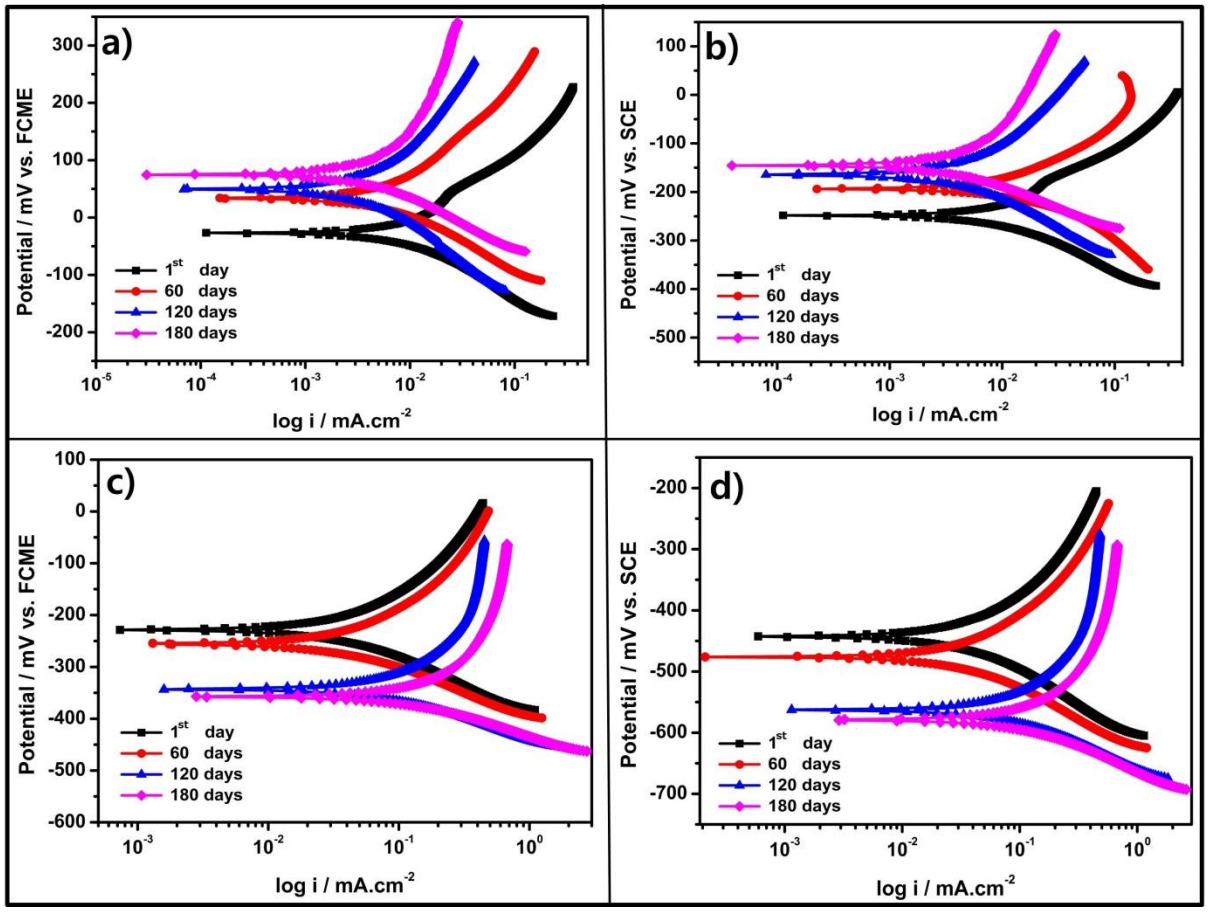

Fig. 4. The Potentiodynamic polarization curve for the steel rebar immersion SCPS with respect to FCME(a); SCE(b) and steel rebar immersion in chloride contaminated SCPS with respect to FCME(c); SCE(d).

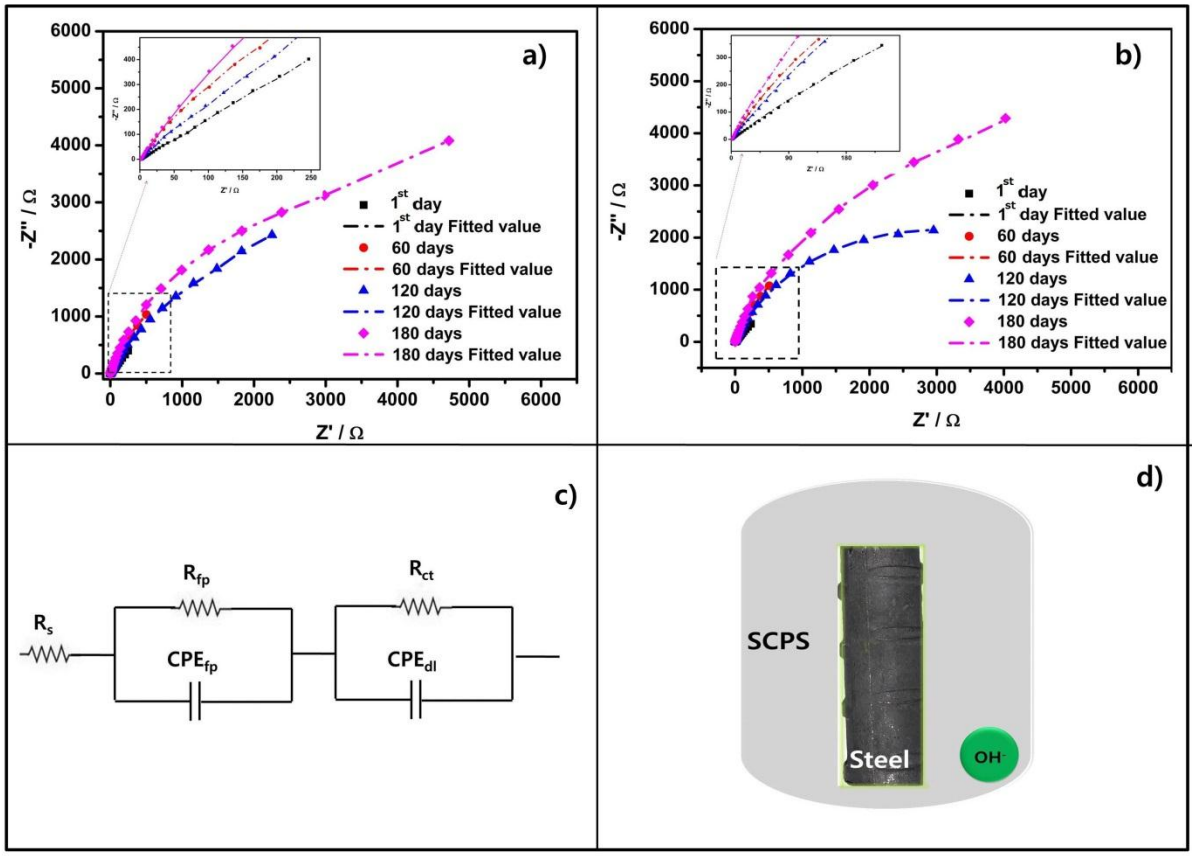

Fig. 5. AC-Impedance plot for the steel rebar immersed in SCPS with respect to FCME(a); SCE(b); equivalent circuit fit (c); and schematic diagram for steel rebar immersion in SCPS.

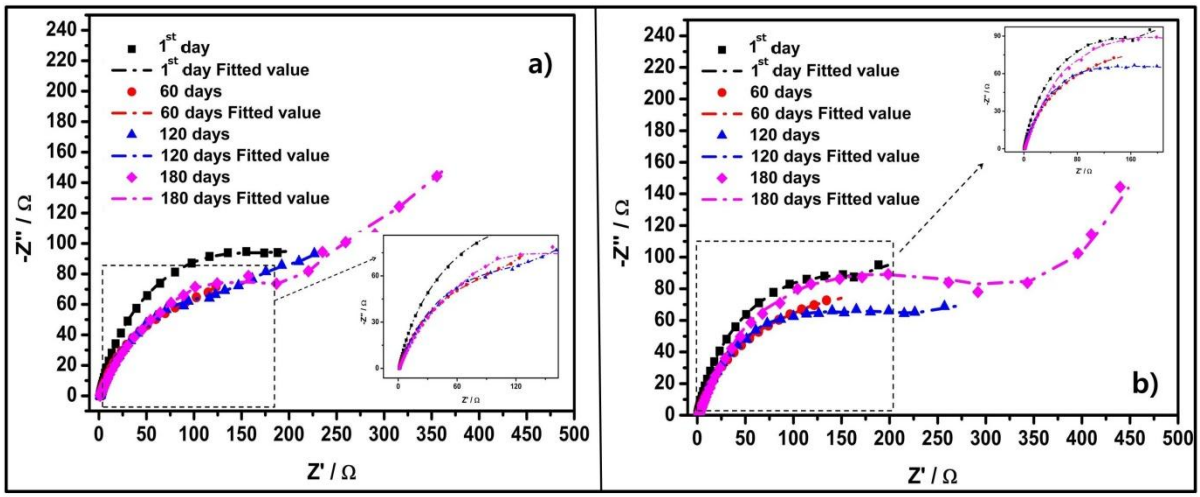

Fig. 6. AC-Impedance plot for steel rebar immersed in chloride contaminated SCPS with respect to FCME(a); SCE(b).

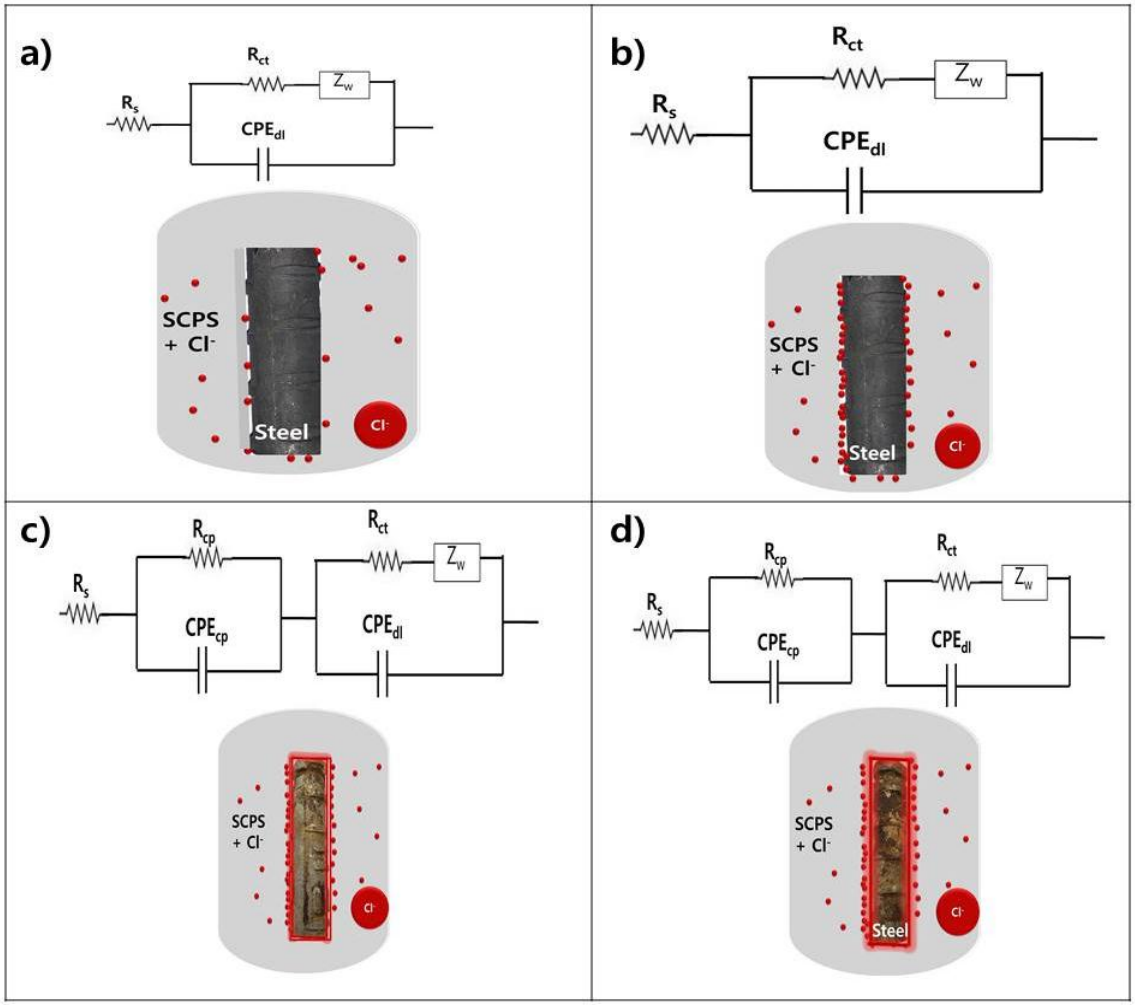

Fig. 7. AC-Impedance plot equivalent circuit and schematic diagram of the steel rebar corrosion in chloride contaminated SCPS with exposure period of 1st day (a); 60 days (b); 120 (c) days; and 180 days (d).

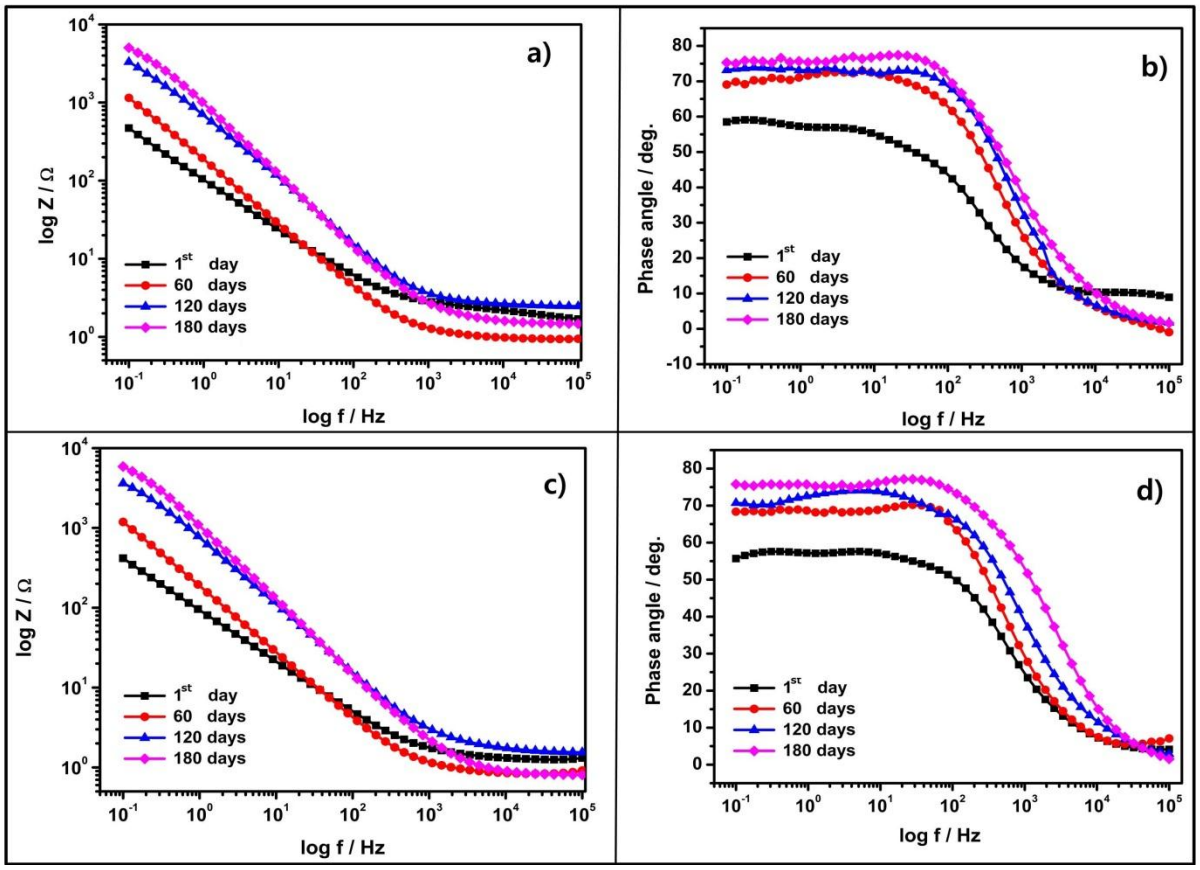

Fig. 8. Impedance modulus plot (a-c) and phase angle (b-d) for the steel rebar immersed in SCPS with respect to FCME (a-b) and SCE(c-d).

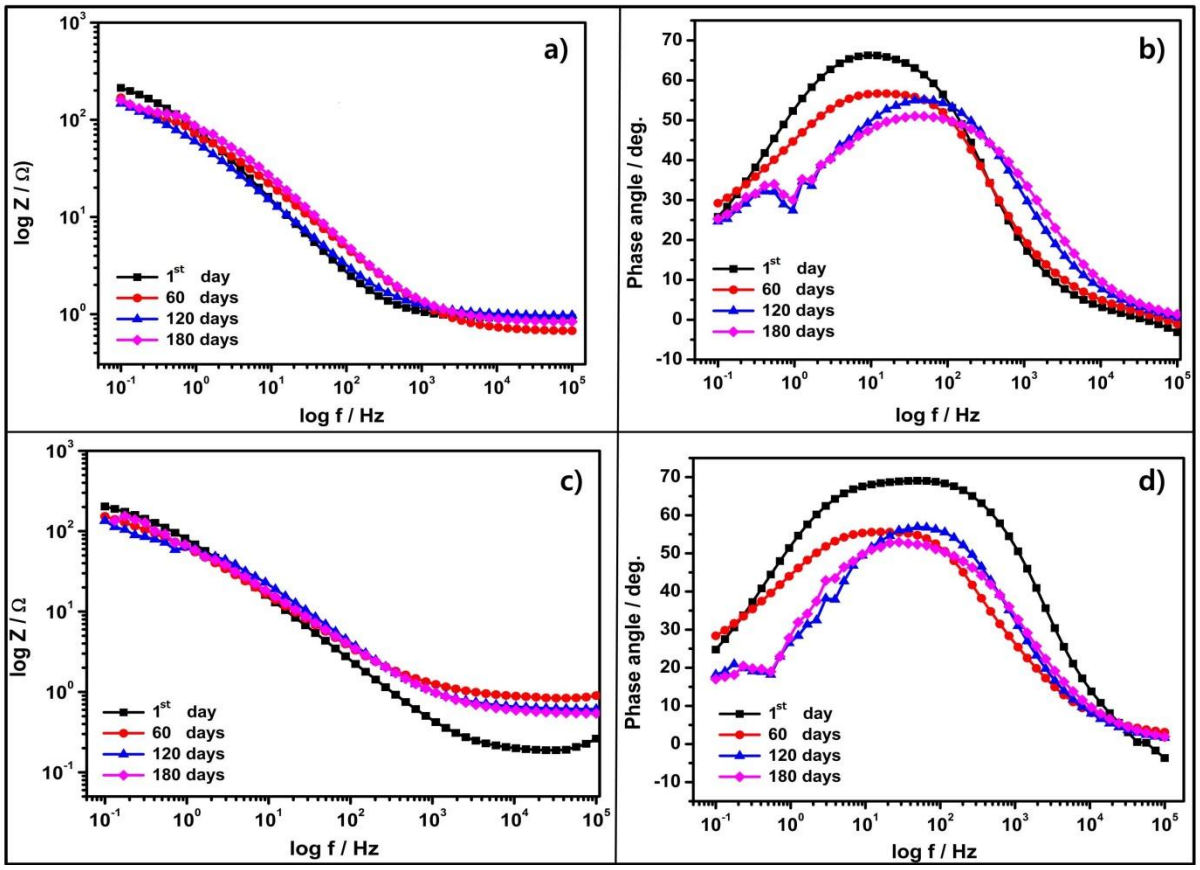

Fig. 9. Impedance modulus plot (a-c) and phase angle (b-d) for the steel rebar immersed in chloride contaminated SCPS with respect to FCME (a-b) and SCE(c-d).

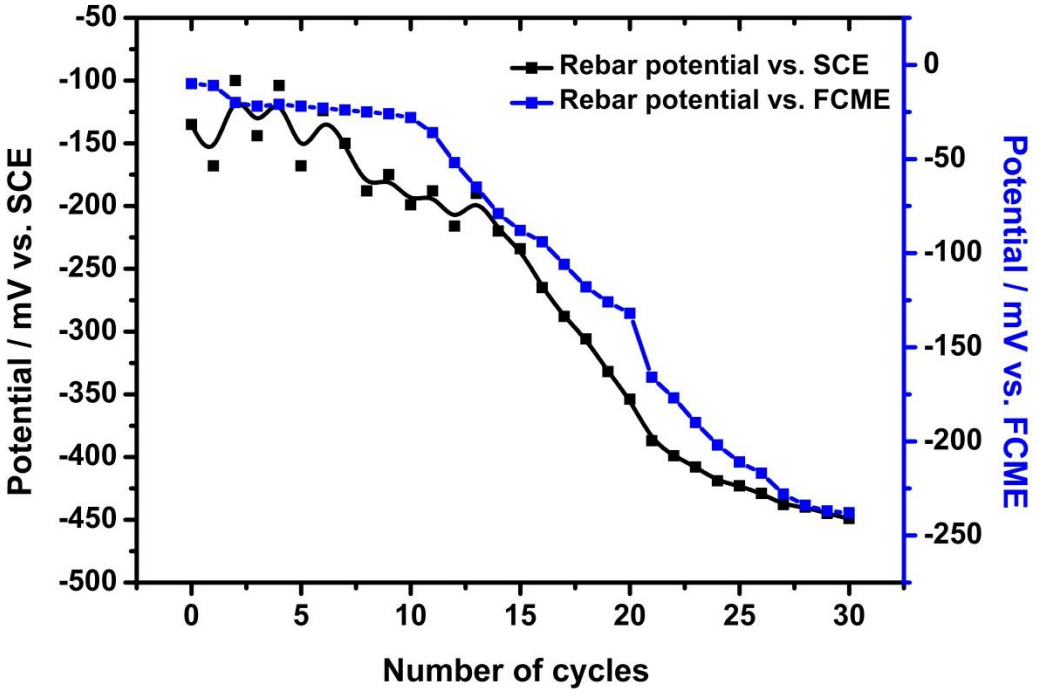

Fig. 10. The OCP of embedded steel rebar in concrete with respect to FCME and SCE for various exposure periods

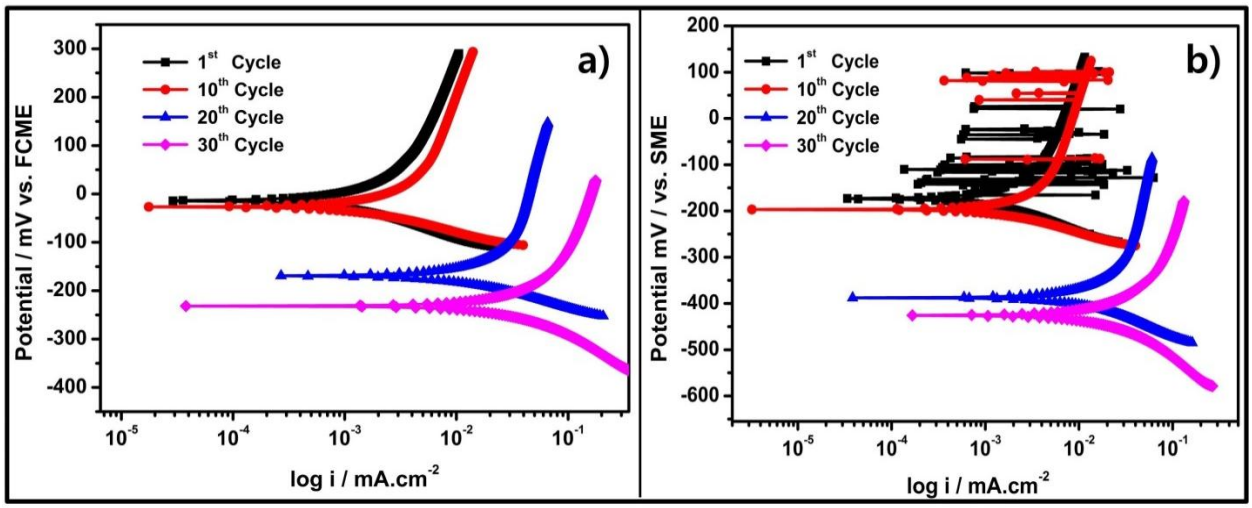

Fig. 11. The potentiodynamic polarization curve for embedded steel rebar in concrete with respect to FCME (a); and SME (b) at various cycles.

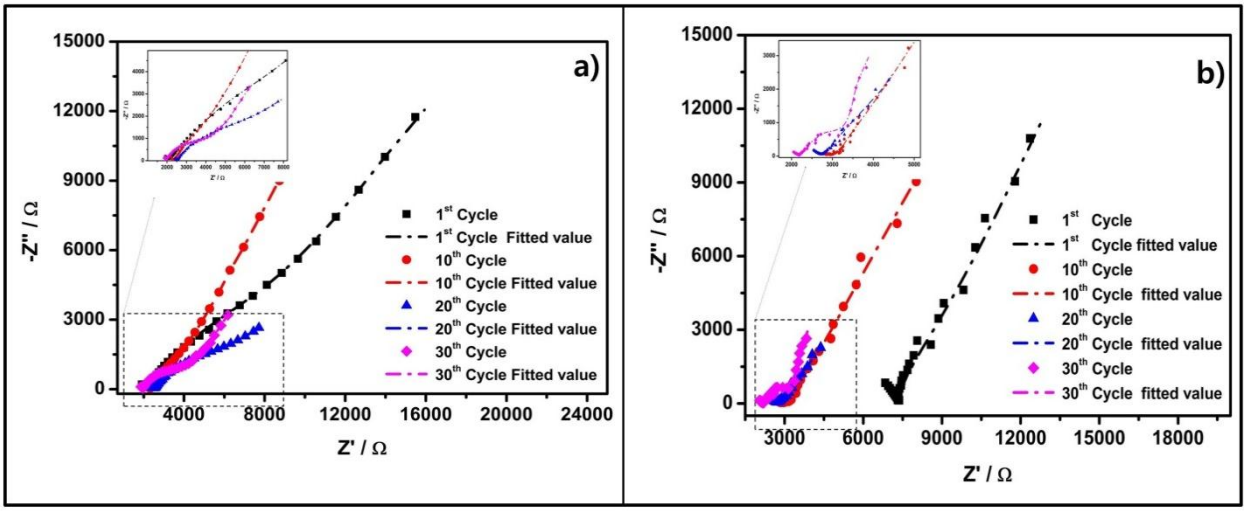

Fig. 12. AC-Impedance plots for the steel rebar embedded in concrete with respect to FCME (a); and SME (b) at various cycles.

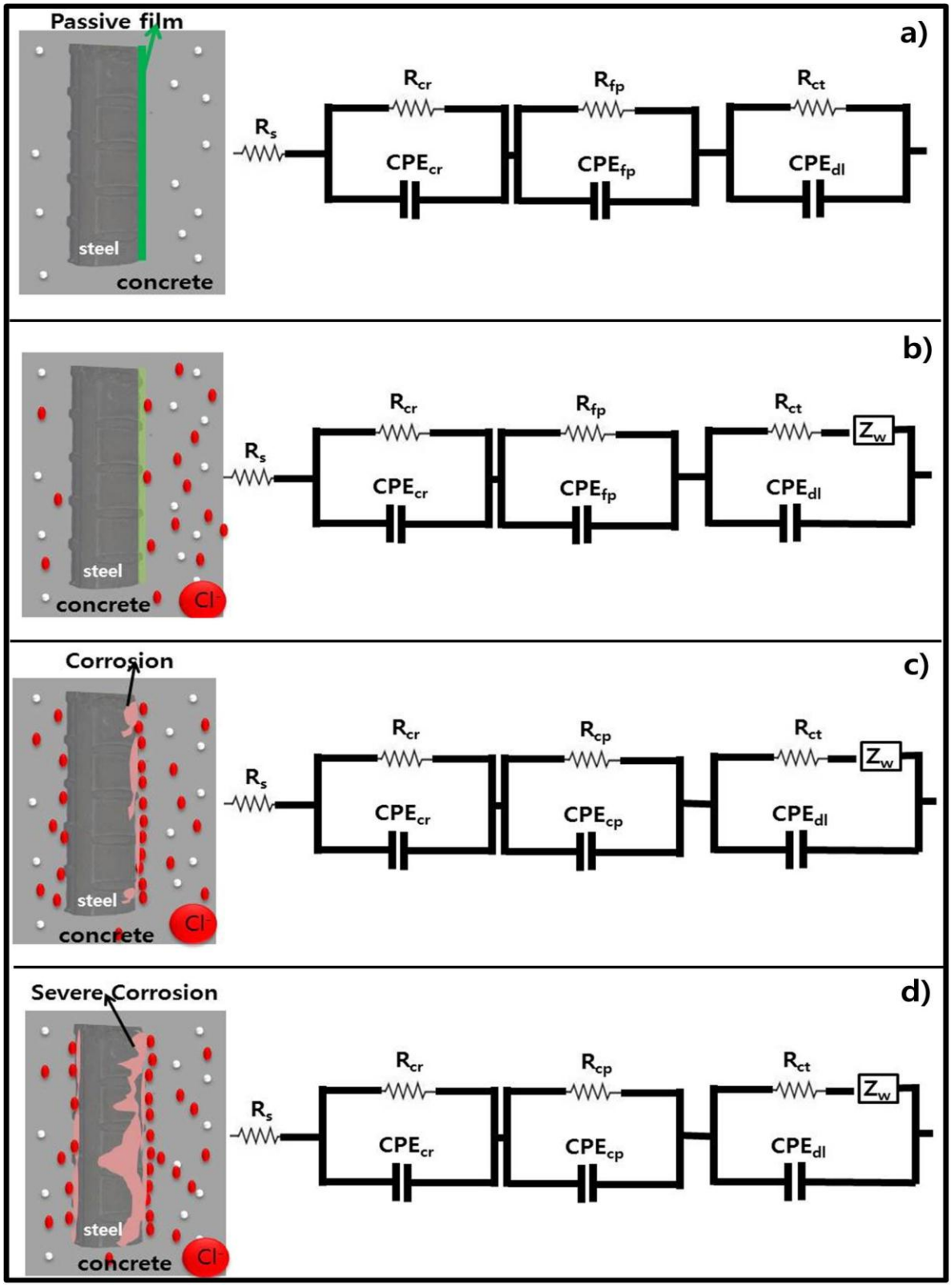

Fig. 13. AC-Impedance plot equivalent circuit and schematic diagram of the steel rebar corrosion in concrete at various 1st (a); 10th (b); 20th (c) and 30th (d) cycles.

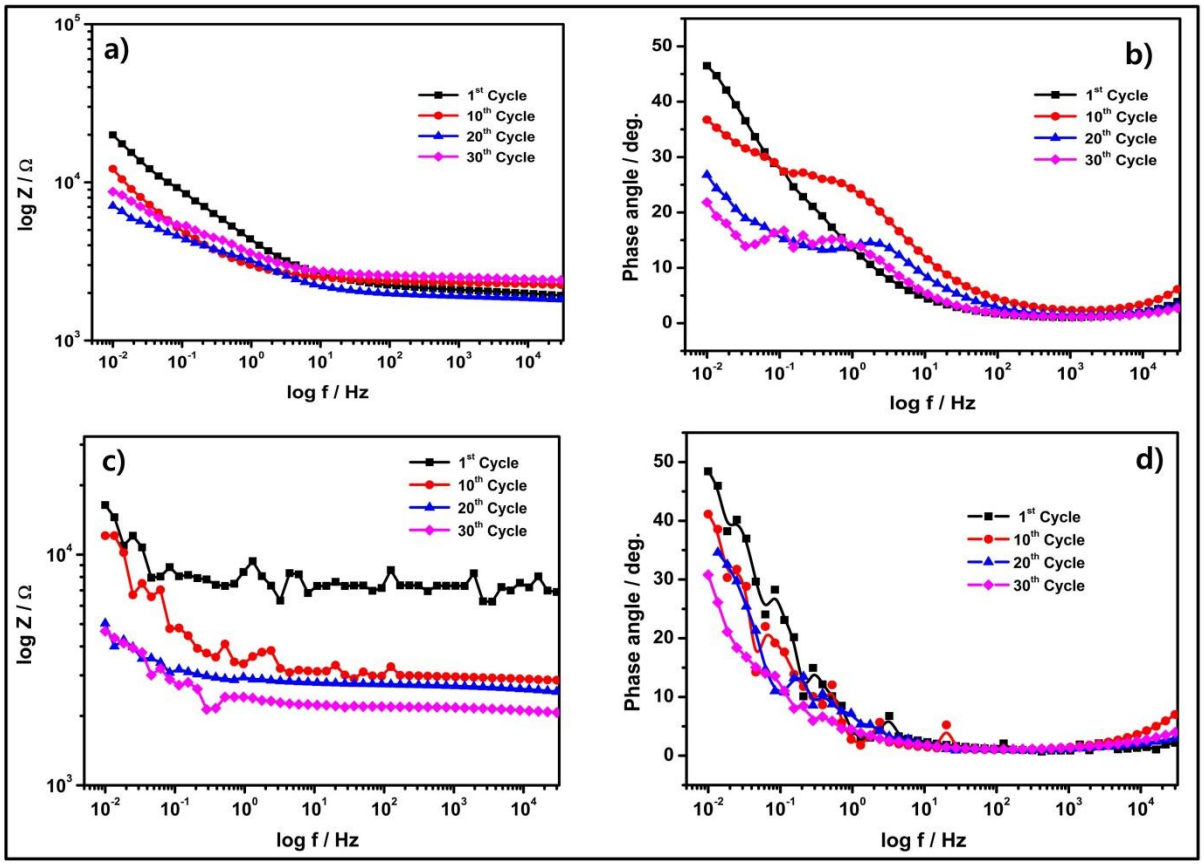

Fig. 14. Impedance modulus plot (a-c) and phase angle (b-d) for the steel rebar embedded in concrete with respect to FCME (a-b) and SME(c-d);

List of Tables

Table 1
Chemical composition of Ordinary Portland cement (OPC).

Types	Chemical composition (mass %)							Physical properties
	SiO_2	Al_2O_3	Fe_2O_3	CaO	MgO	SO_3	LOI	Specific gravity (g/cm^3)
OPC	21.96	5.27	3.44	63.41	2.13	1.96	0.79	3.16

Table 2
Corrosion condition of rebar related to OCP measurement as per ASTM C-876 standards [46] against SCE and FCME.

OCP values (ASTM C876)		OCP values (mV vs FCME) (±10 mV)	Corrosion condition
(mV vs. CSE)	(mV vs. SCE)		
< -500	< -426	-205	Severe corrosion
< -350	< -276	-56	High (< 90% risk of corrosion)
-200 to -350	-126 to -275	+95 to -54	Intermediate corrosion risk
> 200	> -125	> +94	Low (10% risk of corrosion)

* CSE= copper/copper sulphate electrode; SCE= saturated calomel electrode

Table 3
Potentiodynamic polarization parameters for the steel rebar immersion in SCPS with respect to FCME and SCE.

No. of days	vs. FCME			vs. SCE		
	E_{corr} (mV)	I_{corr} (mA.cm^{-2}) × 10^{-2}	Corrosion rate (mmpy) × 10^{-2}	E_{corr} (mV)	I_{corr} (mA.cm^{-2}) × 10^{-2}	Corrosion rate (mmpy) × 10^{-2}
1st	-27.69	1.277	14.79	-248	0.242	14.39
60	33.75	0.6149	7.125	-193	0.970	11.23
120	51.14	0.3650	4.23	-161	0.478	5.54
180	76.25	0.3427	3.971	-145	0.402	4.658

Table 4
Potentiodynamic polarization parameters for the steel rebar immersion in chloride contaminated SCPS with respect to S FCME and SCE.

No. of days	vs. FCME			vs. SCE		
	E_{corr} (mV)	I_{corr} (mA.cm^{-2}) ×10^{-2}	Corrosion rate (mmpy) × 10^{-2}	E_{corr} (mV)	I_{corr} (mA.cm^{-2}) ×10^{-2}	Corrosion rate (mmpy) ×10^{-2}
1st	-228	3.706	42.95	-441	3.070	35.58

60	-254	4.241	49.14	-475	3.528	40.88
120	-337	10.166	117.80	-562	9.7098	112.44
180	-355	14.031	162.59	-576	13.349	154.688

Table 5
AC-impedance parameters for the steel rebar immersion in SCPS with respect to FCME and SCE.

No. of days	R_s ($\Omega.cm^2$)	R_{fp} ($k\Omega.cm^2$)	CPE_{fp} ($\Omega^{-1}\cdot cm^{-2}s^{-n}$) $\times 10^{-3}$	**N**	R_{ct} ($k\Omega.cm^2$)	CPE_{dl} ($\Omega^{-1}\cdot cm^{-2}s^{-n}$) $\times 10^{-5}$	**N**
	vs. FCME						
1st	2.027	0.736	2.272	0.71	2.026	4.410	0.98
60	0.991	0.850	1.179	0.85	2.854	1.0540	0.94
120	2.651	1.047	1.154	0.78	4.750	0.4241	0.90
180	1.541	2.565	1.095	0.85	6.500	0.1254	0.95
	vs. SCE						
1st	1.213	0.775	2.936	0.68	2.076	2.560	0.43
60	0.841	0.854	1.513	0.84	2.954	1.340	0.86
120	1.607	1.090	1.167	0.80	4.847	0.4297	0.91
180	0.839	2.522	1.148	0.88	6.858	0.0958	0.96

Table 6
AC-impedance parameters for the steel rebar immersion in chloride contaminated SCPS with respect to FCME and SCE.

No. of days	R_s ($\Omega.cm^2$)	R_{cp} ($k\Omega.cm^2$)	CPE_{cp} ($\Omega^{-1}\cdot cm^{-2}s^{-n}$) $\times10^{-3}$	N	R_{ct} ($k\Omega.cm^2$)	CPE_{dl} ($\Omega^{-1}\cdot cm^{-2}s^{-n}$) $\times10^{-3}$	N	W ($\Omega\cdot cm^2s^{0.5}$) $\times10^{-2}$
vs. FCME								
1st	0.901	-	-	-	0.210	2.265	0.81	2.0
60	0.969	--	-	-	0.155	3.383	0.72	2.5
120	1.240	0.156	5.910	0.70	0.132	24.09	0.91	8.8
180	1.271	0.207	5.121	0.64	0.143	21.17	0.79	3.3
vs. SCE								
1st	0.186	-	-	-	0.194	2.206	0.57	2.2
60	0.828	-	-	-	0.156	3.404	0.70	2.6
120	1.363	0.132	4.660	0.73	0.122	26.79	0.74	9.3
180	1.554	0.248	4.221	0.66	0.149	21.13	0.78	3.2

Table 7
Potentiodynamic polarization parameters for the steel rebar embedded in concrete with respect to FCME and SCE

No. of cycles	vs. FCME			vs. SME		
	E_{corr} (mV)	I_{corr} ($mA.cm^{-2}$) $\times10^{-2}$	Corrosion rate (mmpy) $\times10^{-2}$	E_{corr} (mV)	I_{corr} ($mA.cm^{-2}$) $\times10^{-2}$	Corrosion rate (mmpy) $\times10^{-2}$
1st	-12.89	0.206	2.387	-174	0.222	2.573
10th	-28.34	0. 268	3.105	-196	0.286	3.314
20th	-165.79	1.93	22.360	-387	1.44	16.680
30th	-218	3.839	44.490	-439	2.744	31.790

Table 8
AC-impedance parameters for the steel rebar embedded in concrete with respect to FCME and SCE

Impedance parameters	No. of cycles							
	vs. FCME				vs. SME			
	1st cycle	10th cycle	20th cycle	30th cycle	1st cycle	10th cycle	20th cycle	30th cycle
R_s ($\Omega.cm^2$)	53.83	25.0	20.98	15.23	85	75.23	22.96	18.23
R_{cr} ($k\Omega.cm^2$)	3.52	3.50	1.63	1.20	8.05	3.907	2.17	2.02
CPE_{cr} $\Omega^{-1}\cdot cm^{-2}s^{-n}$ $\times 10^{-7}$	0.163	0.182	1.24	41.83	0.208	0.504	7.50	30.445
N	0.18	0.85	0.88	0.85	0.18	0.68	0.55	0.25
R_{fp} ($k\Omega.cm^2$)	0.439	0.269	-	-	0.938	0.321	-	-
CPE_{fp} $\Omega^{-1}\cdot cm^{-2}s^{-n}$ $\times 10^{-3}$	1.205	2.435	-	-	4.71	5.301	-	-
N	0.762	0.686	-	-	0.859	0.912	-	-
R_{cp} ($k\Omega.cm^2$)	-	-	-	0.251	-	-	-	0.403
CPE_{cp} $\Omega^{-1}\cdot cm^{-2}s^{-n}$	-	-	-	0.0138	-	-	-	0.0119
N	-	-	-	0.66	-	-	-	0.67
R_{ct} ($k\Omega.cm^2$)	1. 95	1.324	0.562	0.350	2.095	1.50	0.603	0.420
CPE_{dl} $\Omega^{-1}\cdot cm^{-2}s^{-n}$ $\times 10^{-3}$	0.388	3.02	4.414	11.8	0.34	3.31	5.79	15.2
N	0.65	0.70	0.54	0.58	0.79	0.63	0.53	0.99
Z_W $\Omega\cdot cm^2s^{0.5}$ $\times 10^{-3}$	0.392	0.602	2.01	1.99	0.957	0.992	1.43	1.41